JOURNAL OF GEOPHYSICAL RESEARCH, VOL. 102, NO. D14, PAGES 16,619–16,637, JULY 27, 1997

Inhomogeneity effects on cloud shortwave absorption measurements: Two-aircraft simulations

Alexander Marshak,[1] Anthony Davis,[1] Warren Wiscombe, and Robert Cahalan

NASA Goddard Space Flight Center, Climate and Radiation Branch, Greenbelt, Maryland

Abstract. We set up an Observation System Simulation in order to quantify the idiosyncratic uncertainties caused by cloud inhomogeneity in two-aircraft measurements. An independently validated fractal model is used to simulate the horizontal variability of optical depth for boundary layer stratus, with and without gaps. A spectral band between 0.9 and 1.0 μm, with a combination of strong and weak water vapor absorption and negligible weak liquid water absorption, is selected for a detailed study of column absorption. Measurements of upwelling and downwelling radiative fluxes are simulated by the Monte Carlo method at two altitudes in a realistic cloudy atmosphere. We consider three methods of estimating column absorption: cloud forcing ratio, reflectance (R) versus transmittance (T) regression, and Ackerman-Cox correction. Emphasis is on the second method, R versus T, which is shown to be biased in the direction of enhanced absorption as long as the R and T data points are affected by horizontal fluxes. In other words, to reduce the bias to an acceptable level, (R, T) measurements must be at a scale well within the regime where the independent pixel approximation is accurate. Under completely cloudy skies, radiative smoothing processes dominate the bias in the absorption estimate at small scales; hence spatial averages over at least 30 times the radiative smoothing scale, which is commensurate with cloud thickness, are required. If there are substantial gaps in the cloud cover, geometrical shadowing and cloud side-illumination effects overwhelm the radiative smoothing. As a result, the bias in R versus T methodology is worsened, and aircraft positioning becomes more critical. We also examine the effect of Sun angle and instrumental parameters such as vertical separation and horizontal offset between aircraft. The Ackerman-Cox correction offers an alternative to spatial averaging; a modification of this intrinsically small-scale approach that can virtually eliminate horizontal flux contributions in the data is presented.

1. Introduction

Recent analyses of solar radiation measurements below and above clouds suggest that clouds may absorb far more solar shortwave radiation than predicted by standard radiation models [*Cess et al.*, 1995, 1996; *Pilewskie and Valero*, 1995]. To test this hypothesis, Atmospheric Radiation Measurement (ARM) Enhanced Shortwave Experiment (ARESE) measured shortwave fluxes from aircraft at different altitudes as well as multiple sites on the surface, all within ARM's Southern Great Plains facility Cloud and Radiation Testbed (CART) in Oklahoma.

One way to analyze such measurements, popularized by R. Cess [*Cess et al.*, 1995, 1996], is to plot the above cloud reflectance (R) as a function of below cloud transmittance (T). The absolute slope, $-\delta R/\delta T$, of the R versus T scatterplot supposedly characterizes the amount of radiation absorbed by clouds; following *Cess et al.* [1995], we denote this slope $\beta = |\langle \delta R/\delta T \rangle|$. We are concerned that this approach, while working well for idealized horizontally homogeneous clouds, might lead to biases in the case of real, and therefore horizontally inhomogeneous, clouds [*Imre et al.*, 1996, H. Barker and Z.-Q. Li, Interpreting shortwave albedo-transmittance plots: Observations versus models, submitted to *Geophysical Research Letters*, 1997 (hereinafter referred to as Barker and Li, submitted manuscript, 1997)]. We therefore developed an Observation System Simulation based on a Monte Carlo solution of the radiative transfer equation [*Marchuk et al.*, 1980] to investigate this issue.

Column absorption is a combined effect of atmospheric gases, cloud liquid water, and aerosol. In order to minimize the absorption by cloud drops, a spectral band around 0.94 μm with strong molecular and weak liquid absorption has been chosen for detailed analysis. Water vapor distribution is assumed horizontally homogeneous. The only source of three-dimensional (3-D) effects is therefore the horizontal distribution of cloud liquid water, which is simulated using a realistic fractal model of marine stratocumulus (Sc) variability [*Cahalan et al.*, 1994a, *Marshak et al.*, 1994]. For more realism, gaps in the cloud cover were added in a somewhat ad hoc fashion; domain-averaged cloud liquid water amount was held constant for all cloud models while the cloud fraction was varied.

Using a preliminary version of our Observation System Simulation (without gases), *Marshak et al.* [1997a] simulated two-aircraft experiments to study the effects of (1) varying the degree of spatial averaging of upwelling and downwelling fluxes and (2) varying horizontal and vertical offsets between aircraft. As radiation "instruments," they used both 3-D Monte Carlo (MC) and Independent Pixel Approximation (IPA) models [*Cahalan et al.*, 1994b]. Specifically, *Hayasaka et*

[1]Also at Science Systems and Applications, Inc., Lanham, Maryland.

Paper number 97JD01153.
0148-0227/97/97JD-01153$09.00

al.'s [1995] two-aircraft experiment over the North Pacific Ocean was simulated separately for visible and near-infrared wavelengths with no gaseous absorption. The present study incorporates gaseous absorption and goes far beyond the parameter space explored by *Marshak et al.* [1997a].

In another paper [*Marshak et al.*, 1997b], we distinguish between "apparent" absorption, defined as the difference between two net fluxes simulated at fixed altitudes below and above clouds, and "true" column absorption. Apparent absorption contains "true" absorption by water vapor and "pseudoabsorption," traceable to horizontal fluxes excited by the inhomogeneity in cloud structure. We use an enhanced version of our Observation System Simulation (with aerosol and surface albedo added) to show that 3-D radiative transfer processes increase true column absorption only by about 2% relative to IPA computations in the 0.9–1.0 μm spectral band. Extended semiempirically to broadband absorption, this enhancement is not sufficient to explain the discrepancy between measurements and models reported by *Cess et al.* [1995] and others. This argues for alternate mechanisms for absorption enhancement which may or may not involve clouds [*Arking et al.*, 1996; *Arking*, 1996]. However, recent simulations of broken cloudiness (with fixed cloud albedo) using stochastic radiative transfer [*Byrne et al.*, 1996] as well as a detailed broadband case study of a tropical cloud field [*O'Hirok and Gautier*, 1997] indicate that at least part of the enhancement absorption by clouds can be explained by the inhomogeneity of cloud structure. So the role of 3-D transport in (true) absorption remains an open question; in this paper we address purely observational issues.

On the basis of the analysis of domain-averaged column absorption between 0.9 and 1.0 μm by *Marshak et al.* [1997b], we will consider in the following that true absorption is modeled accurately enough within the IPA. This premise enables us to focus more closely on the true versus apparent absorption distinction, with specific experimental methodology in mind. The main points to be discussed are (1) the effect of horizontal fluxes on column absorption estimates based on reflectance versus transmittance linear regression, (2) removal of the effect of horizontal fluxes by spatial averaging, (3) horizontal and vertical offsets between aircraft, (4) the effect of cloud fraction and solar zenith angles, and (5) removal of the effect of horizontal fluxes at relatively small measurement scales by using a modified *Ackerman and Cox* [1981] correction.

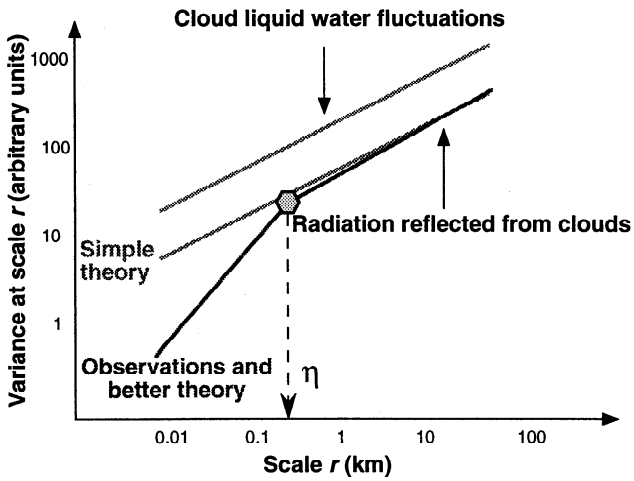

Figure 1. Radiative smoothing. Schematic log-log plot of variance at a given scale versus that scale (e.g., the power spectrum or the second-order structure function). It shows scale-invariant cloud liquid water data and radiation computed in two different ways: Independent Pixel Approximation ("simple theory") and Monte Carlo ("better theory"). The better theory curve shows a scale break at the "radiative smoothing scale" $\eta \approx 200$–300 m for marine stratocumulus (Sc) and agrees with Landsat observations. The simple theory is in one-to-one correspondence with liquid water path; it shows no scale break.

The structure of this paper is as follows. In the next section we briefly discuss the scales that determine the magnitude of the net horizontal fluxes. Section 3 describes our cloud model, simulation techniques, and "measured" fluxes. For deducing the effect of absorption by clouds, cloud radiative forcing ratio and reflectance (R) versus transmittance (T) linear regression are discussed in section 4. Section 5 studies the effect of spatial averaging, solar zenith angle, and cloud fraction on the R versus T slope. In sections 6 and 7 we discuss the effects of vertical and horizontal offsets between aircraft. The results are summarized in section 8. In the Appendix an *Ackerman and Cox* [1981] type correction is modified for the spectral interval 0.9–1.0 μm.

2. Scales of Importance for Horizontal Radiative Fluxes in Single Cloudy Layers

2.1. Partial Cloud Cover: The Cloud Layer Thickness

Under partially cloudy skies, the primary source of horizontal fluxes is oblique illumination directly from the Sun and diffuse reflection off cloud sides. The simplest mental model of broken cloudiness is a single layer of clouds with a characteristic thickness h; clouds are opaque reflective objects with a given size distribution and spaced according to a given intercloud distance distribution. For a given Sun angle θ_0, there is a minimum spacing distance $h \tan \theta_0$ that enables direct sunlight to reach the subcloud layers and ground. By the same token, cloud sides become fully illuminated and reflect a considerable amount of light toward the surface; therefore we can anticipate intense horizontal fluctuations of irradiance (downwelling flux) below cloud as we move from geometrically shadowed areas to directly illuminated ones, with added light from cloud sides. To obtain this variability, we only require that intercloud distance in excess of $h \tan \theta_0$ is not a rare occurrence. In a more accurate conceptualization the clouds are diffusely semitransparent and internally variable. However, this refinement will in general slightly dampen the variability in transmitted irradiance as described above.

In the overall radiative budget, reflected irradiance (upwelling flux) must also be considered, but without the direct component it cannot be as spatially variable as the transmitted component discussed previously. This is especially true as measurement level is increased above the top of the cloudy layer. To summarize, excluding grazing and overhead incidence, the important scale in a broken cloud system with a reasonably broad range of intercloud spacings is commensurate with h.

2.2. Complete Cloud Cover: The Radiative Smoothing Scale

Under completely cloudy skies the only source of horizontal fluxes is the internal variability of the cloud layer. Comparative scale-by-scale analyses [*Davis et al.*, 1994] of

radiation fields computed by both MC and IPA methods show that there is a characteristic scale η, which we have dubbed the "radiative smoothing scale" [*Marshak et al.*, 1995; *Davis et al.*, 1997d; see also *Cahalan*, 1989]. Figure 1 is a schematic illustration of the analyses that led to this discovery. For scales larger than η both IPA and MC radiation fields have the same statistical properties, while for scales smaller than η the MC radiation field has a much smoother behavior, in agreement with 30 m resolution Landsat observations [*Davis et al.*, 1997a]. Scale η thus separates the following two distinct scaling regimes in the radiation reflected (transmitted) from clouds: (1) scales $> \eta$ show structure (hence statistics) similar to that of the cloud liquid water, the one-to-one correspondence being ensured by the IPA, and (2) scales $< \eta$ show radiation fields much smoother than predicted by the cloud structure in the framework of the IPA.

Davis *et al.* [1997a] showed that for reflected radiation,

$$\eta_R \approx h \; / \; [(1-g)\langle\tau\rangle]^{1/2}, \qquad (1a)$$

where values typical of marine stratocumulus (Sc) are $h \approx 300$ m and $\langle\tau\rangle \approx 13$ (the cloud's geometrical and mean optical thicknesses, respectively) and $g = 0.85$ is the scattering phase function's asymmetry factor. These values give $\eta_R \approx 215$ m in good agreement with their analyses of spatial correlations in Landsat images. Interpretation of (1a) is as follows [*Davis et al.*, 1997a]. Suppose all the photons were released into the cloud at the same point. Variance of the horizontal distance ρ they travel before being reflected is $\langle\rho^2\rangle_R \sim h^2/[(1-g)\langle\tau\rangle]$, as shown by *Davis et al.* [1997d] in the frame of diffusion theory. Unsurprisingly, the smoothing scale η_R is found to be commensurate with $\langle\rho^2\rangle_R^{1/2}$.

For transmitted photons we have $\langle\rho^2\rangle_T \sim h^2$ in the photon diffusion limit [*Davis et al.*, 1997d]; accordingly, the smoothing scale for transmitted radiance is close to $\langle\rho^2\rangle_T^{1/2}$ for dense enough clouds [*Davis et al.*, 1997a, b] and

$$\eta_T \approx h\,. \qquad (1b)$$

Together, (1a) and (1b) determine the "overall" radiative smoothing scale η as the greater of η_R and η_T. Since the derivations of both (1a) and (1b) are based on diffusion theory, we can safely assume that $(1-g)\tau > 1$. Thus we have

$$\eta \approx \max\left\{\frac{h}{[(1-g)\langle\tau\rangle]^{1/2}},\, h\right\} = h. \qquad (1c)$$

Following (1c), we will not distinguish from now on between the radiation smoothing scale η and cloud geometrical thickness h, considering both as estimates of the scale at which net horizontal fluxes arise in stratiform clouds. A detailed discussion of horizontal fluxes in marine Sc, including a quantitative prediction, can be found in work by *Davis et al.* [1997b].

3. Model Atmosphere and Simulation Techniques

3.1. Water Vapor and Clouds

There are two atmospheric components in our model: water vapor and cloud liquid water. We selected a narrow spectral band from 0.91 μm to 1.0 μm. This band has insignificant Rayleigh scattering, a large range of transmission, weak liquid water absorption, and incident flux near the peak of the solar spectrum. Water vapor absorption is strong around 0.94 μm and very weak around 0.99 μm; see *Marshak et al.* [1997b] for an illustration. The water vapor distribution is assumed to be horizontally homogeneous; the only source of horizontal variability in our atmospheric model is therefore cloud liquid water.

To simulate the horizontal distribution of optical depth τ, we use a one-dimensional bounded cascade model [*Cahalan et al.*, 1994a]. There are two variability parameters in this model. The first one controls the variance-to-mean ratio of cloud liquid water, while the second one determines its scaling behavior [*Marshak et al.*, 1994]. To simulate typical marine Sc, we set the mean optical depth $\langle\tau\rangle = 13$ and cloud thickness $h = 300$ m, hence mean extinction coefficient $\langle\sigma\rangle = \langle\tau\rangle/h = 43$ km^{-1}.

In addition to internal cloud structure, simulated with a bounded cascade model, we supplement cloud structure with gaps. This is done empirically by linearly transforming optical depth and setting negative values to zero [*Marshak et al.*, 1997b]. For details, see Table 1.

3.2. Simulation Techniques

Two standard techniques are used to compute radiative fluxes and radiances in horizontally inhomogeneous atmospheres: the Independent Pixel Approximation (IPA) and Monte Carlo (MC) simulation. The former treats each pixel as an independent plane-parallel layer; the resulting flux at larger-than-pixel scales is obtained by spatially averaging of individual fluxes. As a result, the domain-averaged IPA flux depends only on the one-point probability distribution of the optical depth field.

The shortcoming of the IPA is that it neglects any net horizontal transport (see Figure 1). Thus IPA is a computational abstraction in which the measured one-point probability distribution of cloud optical properties is inserted into a plane-parallel radiative transfer to produce fluxes and radiances. These IPA fluxes and radiances are not in any sense measurable at a single location. They become useful only

Table 1. Cloud Fractions

N	$\langle\tau_{cloudy}\rangle$	τ_{max}	a	b
1.000	13.00	39.3	0.0	1.0
0.930	13.98	59.1	5.6	1.8
0.777	16.73	74.4	7.9	2.4
0.685	18.98	85.1	9.1	2.8
0.629	20.67	92.8	9.8	3.1
0.562	23.13	103	10.7	3.6

A constant value a is subtracted from $\tau_{overcast}(x) > 0$ ($\langle\tau_{overcast}\rangle = 13$) simulated by a bounded cascade model [*Cahalan et al.*, 1994a]; negative values are set to zero. To restore the amount of liquid water to its former value, the resulting optical depth τ is multiplied by another constant $b > 1$. As a result, $\tau_{broken}(x) = b \max\{\tau_{overcast}(x) - a, 0\}$. Constants a and b are uniquely derived from the desired fractional cloudiness N, total amount of liquid water, and two parameters of bounded model. With more gaps, optical depth of cloudy pixels increases as $\langle\tau_{cloudy}\rangle = \langle\tau_{overcast}\rangle/N$.

when integrated with probability density function (pdf) for a mesoscale region.

In contrast, the MC method is an exact solution of the 3-D radiative transfer equation, thus providing us with an accurate estimate of pixel-averaged fluxes and satellite-level radiances in a given direction. The MC variance reduction technique used in our simulations is discussed by *Marchuk et al.* [1980] and, for specific questions, by *Marshak et al.* [1995]. The MC noise level, connection between pointwise and pixel-averaged fluxes, and stability of the domain-averaged results with respect to different realizations of our cloud models are discussed by *Marshak et al.* [1997b].

For the albedo of marine Sc, *Cahalan et al.* [1994b] found a relatively small (around 1%) difference between domain-averaged IPA and MC fluxes. However, as a result of neglecting net horizontal fluxes by IPA, there is a large difference between IPA and MC fluxes in individual pixels [*Cahalan et al.*, 1994b, *Marshak et al.*, 1995; *Titov*, 1997). While the horizontal fluctuations of IPA fluxes follow those of optical depth, the MC fluxes are relatively independent of local optical depth, because of horizontal photon transport. This decoupling of fluxes and optical depth can be in the sense of a smoothing (as in Figure 1) or an enhanced variability (as we now show).

3.3. Simulated Fluxes and Radiances

For different solar zenith angles and different cloud fractions we simulate downwelling radiative fluxes at the top of atmosphere (TOA) (100 km), upper aircraft (5 km), cloud bottom (1 km), lower aircraft (0.5 km), and surface, and their upwelling counterparts at TOA, upper aircraft, cloud top (1.3 km), and lower aircraft. In addition, using local estimation [*Marchuk et al.*, 1980, *Marshak et al.*, 1995], we simulate satellite nadir-radiance measurements. Figure 2 illustrates four downwelling fluxes and three upwelling ones (upwelling flux at below-cloud aircraft is identically zero, since surface albedo $\alpha_s = 0$). The optical depth distribution with cloud fraction $N = 0.777$ is added for reference.

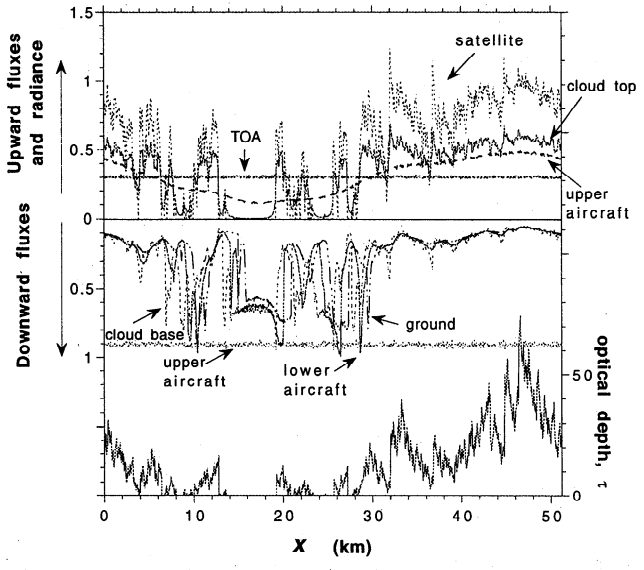

Figure 2. "Measured" radiation fields computed by MC. Cloud fraction $N = 0.777$, solar zenith angle $\theta_0 = 60°$. Upward fluxes at the top of atmosphere (100 km), upper aircraft (5 km) and cloud top (1.3 km). Downward fluxes at upper aircraft, cloud base (1.0 km), lower aircraft (0.5 km) and surface. Nadir radiance measured at satellite level and the simulated horizontal distribution of cloud optical depth are added for reference.

In contrast to the cloud top flux, which follows the variability of cloud optical depth at least for scales larger than the radiative smoothing scale η (Figure 1 and equation (1c)), the flux field sampled by the upper aircraft is much smoother. Indeed, the upward fluxes computed 3.7 km above cloud top are smoothed by contributions from at least 260 pixels or 13 km on average ($3.7 \times \tan(60°) \times 2 \approx 13$ km); thus only large-scale variability of optical depth affects the upper level fluxes [*Barker*, 1995]. This geometrical averaging is even stronger at TOA, where we see a straight line as a result of contributions from thousands of pixels. However, nadir-viewing radiance at satellite level retains the imprint of the fluctuations of cloud optical depth to an extent determined by 3-D radiative transport effects [*Davis et al.*, 1997a].

Horizontal fluxes tend to smooth the reflected radiation fields, but they can easily enhance the variability of their transmitted counterparts, with respect to IPA predictions. As illustrated in Figure 2, this only requires the presence of gaps in the cloud cover. Bearing this in mind, downwelling fluxes at the ground and lower aircraft are substantially smoother than their cloud base counterparts only at high optical depths (e.g., see horizontal locations in Figure 2 between 0 and 5 km, as well as 30 and 50 km). In the low optical depth regions and near cloud edges the variability of all three below cloud downwelling fluxes (cloud base, lower aircraft, and surface) are very close; the spikes at the right cloud edges are only shifted with respect to the distance from cloud base. This shift affects the optimal vertical offset between aircraft for cloud absorption estimations, as discussed in section 6.

4. Methods for Defining the Effect of Clouds on Absorption

We will use two methods, although in quite different ways, for deducing the effect of clouds on column atmospheric absorption of solar radiation. The first is the more traditional and uses the ratios of solar cloud forcing above and below clouds [*Ramanathan et al.*, 1995; *Harshvardhan et al.*, 1996, *Imre et al.*, 1996]. (The solar radiative forcing is usually computed for broadband 0.3–4 μm; recall that here we focus only on 0.9–1.0 μm spectral interval.) The second method uses the slope of the solar reflectance (R) versus transmittance (T) regression [*Cess et al.*, 1995; *Pilewskie and Valero*, 1995; *Li and Moreau*, 1996]. These methods use space and/or time averages and/or least-squares fitting; in this respect, they rely strongly on statistical procedures to remove the spurious effects of spatial variability of cloud cover in column absorption estimates. A third method, Ackerman-Cox correction, takes a contrastingly deterministic approach, exploiting multispectral information; it is discussed in the Appendix.

4.1. Cloud radiative forcing

Cloud radiative forcing above cloud layer, CF^{above}, is defined as the difference between all sky and clear sky (the same atmosphere but with the clouds removed) in net fluxes F,

$$CF^{\text{above}} = F^{\text{above}}_{\text{allsky}} - F^{\text{above}}_{\text{clear}}, \qquad (2a)$$

where net fluxes $F^{\text{above}}_{\text{allsky}}$ and $F^{\text{above}}_{\text{clear}}$ are the difference between downwelling and upwelling fluxes; that is,

$$F^{\text{above}}_{\text{allsky}} = F^{\text{above}\downarrow}_{\text{allsky}} - F^{\text{above}\uparrow}_{\text{allsky}} \tag{2b}$$

$$F^{\text{above}}_{\text{clear}} = F^{\text{above}\downarrow}_{\text{clear}} - F^{\text{above}\uparrow}_{\text{clear}} \tag{2c}$$

Similarly,

$$CF^{\text{below}} = F^{\text{below}}_{\text{allsky}} - F^{\text{below}}_{\text{clear}} \tag{3a}$$

with

$$F^{\text{below}}_{\text{allsky}} = F^{\text{below}\downarrow}_{\text{allsky}} - F^{\text{below}\uparrow}_{\text{allsky}} \tag{3b}$$

$$F^{\text{below}}_{\text{clear}} = F^{\text{below}\downarrow}_{\text{clear}} - F^{\text{below}\uparrow}_{\text{clear}} \tag{3c}$$

The cloud radiative forcing ratio,

$$\beta_{CF} = \frac{CF^{\text{above}}}{CF^{\text{below}}}, \tag{4}$$

characterizes the column absorption between two levels above and below clouds. Indeed, it is easy to show that

$$CF^{\text{above}} = CF^{\text{below}} + A_{\text{allsky}} - A_{\text{clear}}; \tag{5}$$

thus

$$\beta_{CF} = 1 + \frac{A_{\text{allsky}} - A_{\text{clear}}}{CF^{\text{below}}} \tag{6}$$

where A_{allsky} and A_{clear} are the all-sky and the clear-sky column absorptions between two aircraft, respectively. Obviously, $\beta_{CF} = 1$ implies $A_{\text{allsky}} = A_{\text{clear}}$; i.e., no change in column absorption with the addition of a cloud layer. With this definition, $\beta_{CF} < 1$ implies that clouds increase absorption, while $\beta_{CF} > 1$ indicates a loss in column absorption with the addition of cloud layer.

Equations (2)–(6) are simplified if we assume no aerosol and surface albedo $\alpha_s = 0$. Then

$$CF^{\text{above}} = -F^{\text{above}\uparrow}_{\text{allsky}}, \tag{7}$$

$$CF^{\text{below}} = F^{\text{below}\downarrow}_{\text{allsky}} - F^{\text{below}\downarrow}_{\text{clear}} \le 0, \tag{8}$$

and

$$\beta_{CF} = \frac{F^{\text{above}\uparrow}_{\text{allsky}}}{F^{\text{below}\downarrow}_{\text{clear}} - F^{\text{below}\downarrow}_{\text{allsky}}}. \tag{9}$$

We denote $F^{\text{above}\uparrow}_{\text{allsky}}/F^{\text{above}\downarrow}_{\text{allsky}}$ by reflectance R, $F^{\text{below}\downarrow}_{\text{allsky}}/F^{\text{above}\downarrow}_{\text{allsky}}$ by transmittance T, and $F^{\text{below}\downarrow}_{\text{clear}}/F^{\text{above}\downarrow}_{\text{allsky}}$ by clear-sky transmittance T_{clear}, that is,

$$\beta_{CF} = \frac{\langle R \rangle}{\langle T_{\text{clear}} - T \rangle}, \tag{10}$$

where $\langle\ \rangle$ denotes domain averaging.

An alternative way to define the cloud radiative forcing ratio is the inverse of β_{CF} [*Ramanathan et al.*, 1995]. However, we will follow the definition (6); this allows us to directly compare β_{CF} with the one defined by the linear regression of reflectance above clouds versus transmittance below clouds.

4.2. *R* versus *T* Regression

Another way to estimate the effect of clouds on column absorption is to use the R versus T regression [*Cess et al.*, 1995, 1996]. This method eliminates the need for clear-cloud discrimination that can be a major source of uncertainties [*Arking et al.*, 1996; *Arking*, 1996; *Imre et al.*, 1996]. The absolute slope of the R versus T scatterplot, $-\delta R/\delta T$, supposedly characterizes the amount of radiation absorbed by clouds. Let us define β_{LIN} as

$$\beta_{\text{LIN}} = \left| \left\langle \frac{\delta R}{\delta T} \right\rangle_{\text{least squares}} \right|. \tag{11}$$

If one assumes a linear relationship between R and T ($R = a + bT$) and furthermore, that the same regression holds for clear sky ($T_{\text{clear}} = -a/b$), then it follows that $-b = \beta_{\text{LIN}} = \beta_{CF}$. As the simplest example, consider a conservatively scattering atmosphere without gaseous absorption; this yields

$$R = 1 - T, \tag{12}$$

thus $\beta_{\text{LIN}} = \beta_{CF} = 1$. In all other cases we can say that, at best, $\beta_{\text{LIN}} \approx \beta_{CF}$.

As discussed by *Imre et al.* [1996], the strongest assumption for the equality $\beta_{\text{LIN}} = \beta_{CF}$ is that the "all-sky" linear regression between R and T should be identical to the one for clear sky. Imre et al. found that the data used in their analysis (ARM April 1994 data) do not support this assumption. However, in our numerical simulations with a fixed solar zenith angle during a flight and horizontally homogeneous water vapor, aerosol, and surface albedo, the range of the clear-sky pairs (T_{clear}, R_{clear}) reflects only the level of numerical noise. As a result, we have at best an ill-defined problem, and any slope can be assigned to this cluster of points.

4.3. IPA Estimates of β_{LIN} and β_{CF}

Figure 3 illustrates scatterplots of R versus T for solar angle $\theta_0 = 60^\circ$ and three different altitudes: between cloud top and base, between upper and lower aircraft, and between TOA and surface. For simplicity, all fields are computed using MC code. In order to neglect any interactions between pixels, and require aircraft to "see" only a single pixel, the horizontal IPA pixels are made huge (5000 km). Obviously, these IPA fluxes are primarily of theoretical interest, as there is no obvious means of measuring them.

The width of R versus T lines indicates the level of MC noise (about 1-2%). Besides MC noise we see a linear relationship between R and T. As a result, the slopes β_{LIN} are very close to β_{CF} computed using (10). The difference between β_{LIN} and β_{CF} is much less than 1%; this is consistent with the level of MC noise.

Note that

$$\beta(R_{\text{above}}\&T_{\text{below}}) < \beta(R_{\text{cloud}}\&T_{\text{cloud}}) < 1 < \beta(R_{\text{TOA}}\&T_{\text{ground}}), \tag{13}$$

where β is either β_{LIN} or β_{CF}. To understand (13), we use (6), where $CF^{\text{below}} \le 0$. Thus $\beta < 1$ indicates an increase in column absorption with the addition of cloud layer, while $\beta > 1$ indicates a loss. As a result, for solar angle $\theta_0 = 60^\circ$ the addition of a cloud layer increases column absorption between two aircraft and decreases the total column absorption between TOA and surface. This is because of the photon mean path length for cloudy sky between clouds and surface and low solar

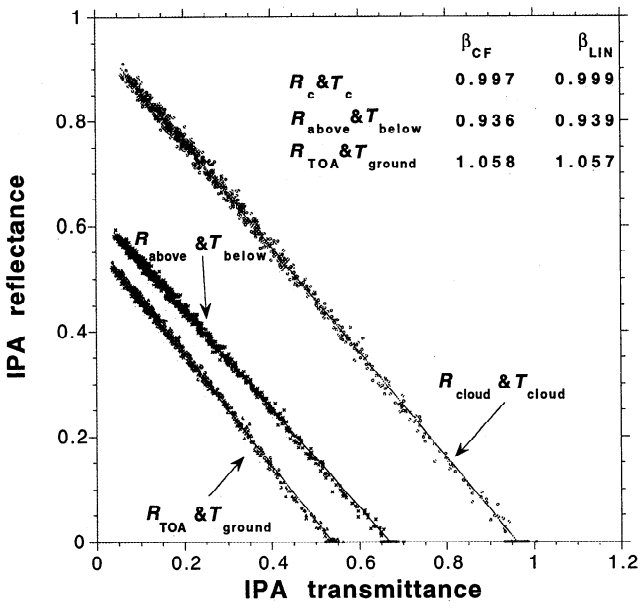

Figure 3. IPA reflectance versus transmittance with linear regressions. Cloud fraction $N = 0.777$, solar zenith angle $\theta_0 = 60^o$. Three different altitudes for R and T: R at TOA (100 km) and T at surface; R at upper aircraft (5 km) and T at lower aircraft (0.5 km); R at cloud top (1.3 km) and T at cloud base (1.0 km). All IPA fields are the result of MC calculations with 5000 km pixel size. The width of R versus T lines indicates the level of MC noise at pixel scales (about 1–2%). β_{CF} and β_{LIN} are computed using (10) and (11), respectively.

elevations is shorter than its clear-sky counterpart; note that water vapor is denser at the lowest levels.

To summarize, both methods for determining the effect of absorption by clouds give the same result if photon horizontal transport is neglected (IPA). At least in the spectral interval between 0.9 and 1.0 μm the value of the resulting ratio (or slope) β strongly depends on the vertical level of measurements and solar angle; these ratios can be either lesser or greater than 1.

This means that changes in β_{CF} do not necessarily characterize the effect of clouds on atmospheric absorption. In addition to the dependence of β_{CF} on measurement levels and solar angles, *Li and Moreau* [1996] showed that β_{CF} depends on cloud height, vertical distribution of water vapor, and surface conditions. On the other hand, *Li et al.* (1995) pointed out that β_{CF}, as the ratio of two numbers, leads to meaningless results if both numbers are relatively small. In the remainder of this R versus T study however, β_{CF}, defined in (10) (assuming the experimentally ideal situation of complete sampling and overall averaging), will be used as a benchmark for the linear regression slope β_{LIN}, defined in (11).

5. MC Estimates of β_{LIN}

5.1. Spatial Averaging

Let

$$\varphi_i = \varphi(x_i),\ x_i = \ell i \quad (i = 1,\ldots,n) \tag{14}$$

represent an average flux value over a pixel size ℓ (0.05 km), the smallest resolution (inner scale) in our numerical experiment. Here $\ell n = L$ (51.2 km) is the outer scale or the size of the basic cloud cell, assuming that cyclical boundary conditions ($\varphi_k = \varphi_{k+n}$, $k \in Z$) are applied.

Next we average φ_i over scale $\ell \le r \le L$, as

$$\phi_j(r) = \frac{\ell}{r} \sum_{i=j}^{j+r/\ell-1} \varphi_i,\ (j = 1,\ldots,n) \tag{15}$$

where we assume for simplicity that r/ℓ is integer. Note that $\phi_j(\ell) = \varphi_j$, while $\phi_j(L) \equiv \phi(L)$ is the domain-averaged value, independent of j. The averaging in (15) is overlapping; as a result, for all scales r we have the same number of points n. In the case of nonoverlapping spatial averaging, the number of points decreases as fast as $n\ell/r$, and for large scales $r > 10$ km

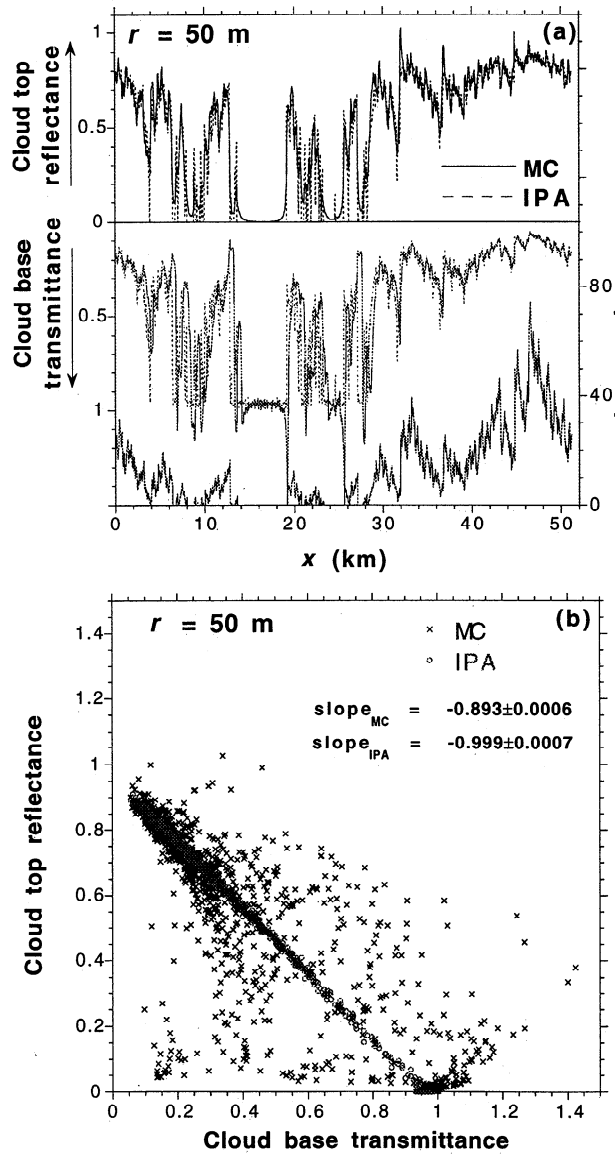

Figure 4. IPA and MC reflectance at cloud top and transmittance at cloud base at the smallest resolution (0.05 km). Cloud fraction $N = 0.777$, solar zenith angle $\theta_0 = 60^o$. (a) IPA and MC reflectance and transmittance fields; optical depth field added for reference. (b) Cloud top reflectance versus cloud base transmittance for MC (crosses) and IPA (circles). For linear regression it is assumed that reflectance and transmittance have the same standard deviation.

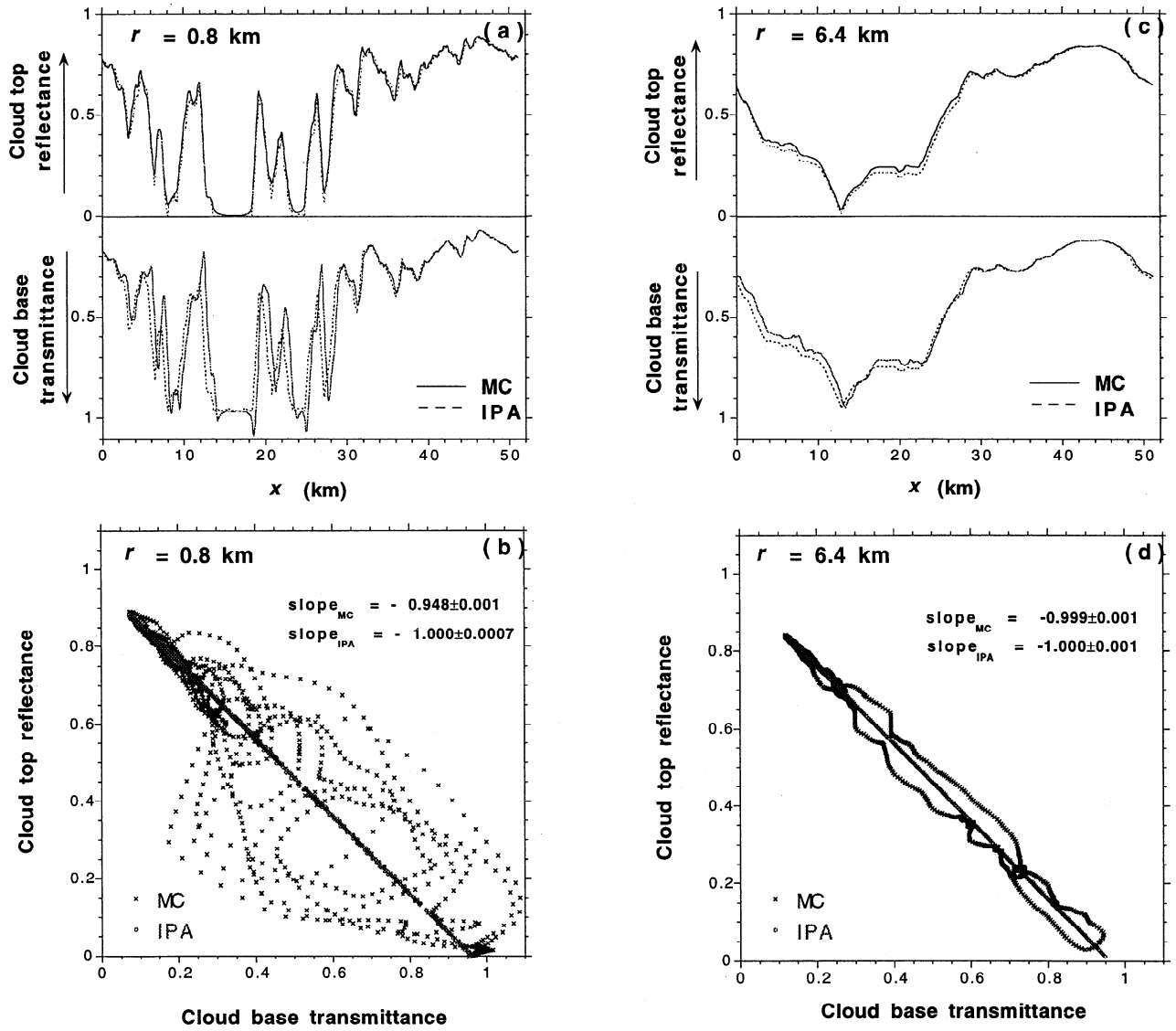

Figure 5. Spatial average of the data in Figure 4. (a) IPA and MC reflectance and transmittance fields averaged over 0.8 km. (b) Cloud-top reflectance versus cloud-base transmittance for MC and IPA averaged over 0.8 km. (c) The same as in Figure 5a but averaged over 6.4 km. (d) The same as in panel (b) but averaged over 6.4 km.

($r > L/4$) we have only four points left, which makes our linear regression less reliable.

5.2. The Effect of Spatial Averaging

Figure 4a illustrates both the IPA and MC fields simulated at cloud top and base. Because of the effect of net horizontal fluxes, MC albedo is smoother than its IPA counterpart. This is also true for transmittance but only for large optical depths. At the edge of the cloud gaps we see strong spikes that indicate bright spots in the locally broken cloud cover. As a result, we have more scatter (Figure 4b) at small optical depths, thus small albedos. This yields a systematically smaller slope β_{LIN} in the R versus T regression (compare $\beta_{LIN} = 0.893$ for MC with $\beta_{LIN} = 0.999$ for IPA). It is assumed that reflectance and transmittance have the same standard deviation σ (MC noise level), and the *Press et al.*'s [1993] routine FITEXY is used to minimize $\sum_1^n (a + bT_i - R_i)^2/(1 + b^2)$.

It is expected that spatial averaging cancels the effect of net horizontal fluxes and reduces the scatter at small optical depths. Indeed, Figure 5a shows both IPA and MC fields averaged over $r = 0.8$ km according to (15) with $r/\ell = 16$ pixels. We see that the effect of cloud edges becomes smaller; hence β_{LIN} increases (Figure 5b). Finally, after averaging over 6.4 km (128 pixels), MC and IPA fields are almost indistinguishable (Figure 5c) and β_{LIN} gives the desired slope, i.e., $\beta_{LIN}(MC) = \beta_{LIN}(IPA) = \beta_{CF}$ (Figure 5d).

To summarize, spatial averaging removes 3-D radiative transfer effects that are characterized by net horizontal fluxes. Besides spatial averaging, the effect of horizontal fluxes on column absorption can also be removed assuming a linear relationship between apparent absorptions in a nonabsorbing spectral region and in the whole near-infrared region [*Ackerman and Cox*, 1981]. An application of this procedure to the spectral interval 0.9–1.0 μm is discussed in the Appendix.

5.3. The Effect of Cloud Fraction

In this section we compare results for different cloud fractions N. With more gaps, redistribution of cloud liquid water increases optical depth of cloudy sky, noting that the same total liquid water is used in all cases.

In Figure 6a we plotted slopes of cloud top reflectance (R) versus cloud base transmittance (T) against different scales r of spatial averaging in (15) for overcast sky (N = 1.000) and broken clouds (N = 0.777). The horizontal line corresponds to the IPA results, which do not depend on spatial averaging. The overall increasing curves contain MC results.

The overcast-sky curve shows three distinct regimes that are naturally characterized in terms of the radiative smoothing scale η: small scales ($r < \eta$), where β_{LIN} is roughly constant but wrong; a transition range ($\eta < r < 20\eta$), where it is rising rapidly; and the largest scales ($r > 20\eta$), where MC and IPA results agree reasonably well and β_{LIN} is constant. Only in the last case does β_{LIN} correctly characterize cloud absorption, that is, $\beta_{LIN}(MC) \approx \beta_{LIN}(IPA) \approx \beta_{CF}$.

The broken cloud case is more complex since 3-D radiative transfer effects of horizontal fluxes are characterized by both radiative smoothing (at large optical depths embedded in extended cloudy areas) and geometrical shadowing (around clear-sky gaps). Geometrical shadowing will always dominate at small scales [cf. *Evans*, 1997]; as a result, the overcast case (N = 1.000) yields β_{LIN} = 0.97 before averaging, while the case N = 0.777 yields β_{LIN} = 0.89. This is because of spikiness in the transmittance field in Figures 4a and b. The large-scale behavior is similar for both cases; since the IPA slopes are almost indistinguishable, both curves converge to the same value of $\beta_{LIN}(IPA)$. Furthermore, the IPA regime is reached at roughly the same scale (6–10 km $\approx$ 20–30η) independently of cloud fraction N, as expected from the characterization of strong shadowing in section 2.1 and recalling from section 2.2 that $\eta \approx h$. This is confirmed by four other cloud fractions from Table 1 plotted in Figure 6b.

From the other hand, we see that the small-scale behavior is very different. Out of six cloud fractions, $\beta_{LIN}(N)$ reaches its minimum at N = 0.930. This is because of a number of small gaps and thus of spikiness in the transmittance, which are responsible for making the R versus T slope flatter. As cloud fraction decreases, the (absolute) small-scale slope increases, returning to the theoretical value of $R(\tau=\infty)/T_{clear}$, which is $\approx$ 1 for small N (Figure 6c). This is because of a cluster of points around R = 0 and $T = T_{clear}$ and also a few points at $R \approx R(\tau=\infty)$ and T =0. The value $\tau = \infty$ is taken to illustrate the fact that since the total liquid water is held fixed, the decrease in the total number of cloudy pixels is compensated by the large optical depths of the remaining cloudy pixels. It is of interest that in the limit of small cloud fractions, $\beta_{LIN} = \beta_{CF}$. Indeed, with all but one point concentrated around (0, T_{clear}) and one point sitting in ($R(\tau=\infty)$, 0), $\beta_{LIN} = R(\tau=\infty)/T_{clear}$. However, it follows from Eq. (10) that β_{CF} is also equal to $R(\tau=\infty)/T_{clear}$, since $\langle R \rangle = R(\tau=\infty)$ and T = 0.

5.4. The Effect of Solar Zenith Angle

Figure 7 shows the absolute least-squares slopes β_{LIN} for four solar angles and cloud fraction N = 0.777. We see that the IPA regime at large scales substantially depends on solar zenith angle; the higher the Sun the smaller $\beta_{LIN}(IPA) \approx \beta_{CF}$. This is understandable, since β is a measure of how much less radiation is absorbed by water vapor between 1 and 1.3 km

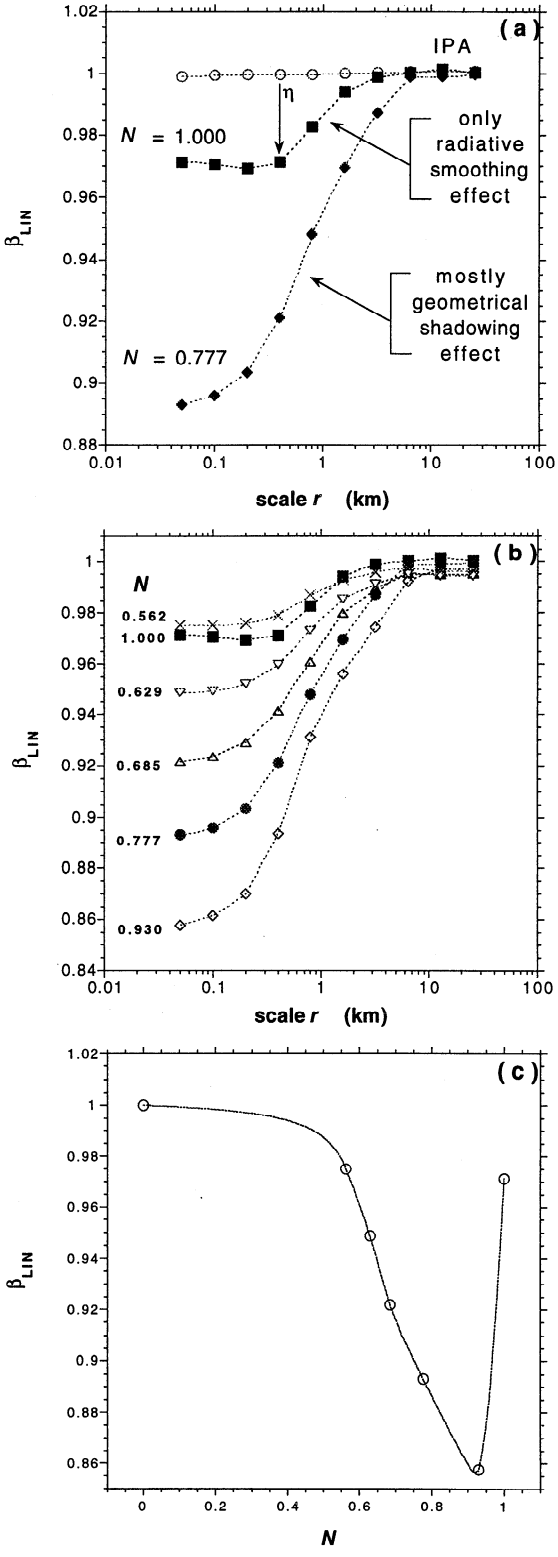

Figure 6. The effect of cloud fraction on measurements at cloud top and cloud base. Solar zenith angle $\theta_0 = 60^0$. (a) The absolute least squares slopes β_{LIN} for both MC and IPA calculations spatially averaged over scale r (from 50 m to 25.6 km). Overcast sky (N = 1.000) and broken clouds (N = 0.777). (b) Six different cloud fractions are used: N = 1.000, 0.930, 0.777, 0.685, 0.629 and 0.562 (see Table 1). The overcast sky and the case of N = 0.777, plotted in Figure 6a, are highlighted with solid squares and circles, respectively. (c) An interpolation between six calculated slopes at the smallest scale from Figure 6a and one hypothetical slope (at N = 0.0).

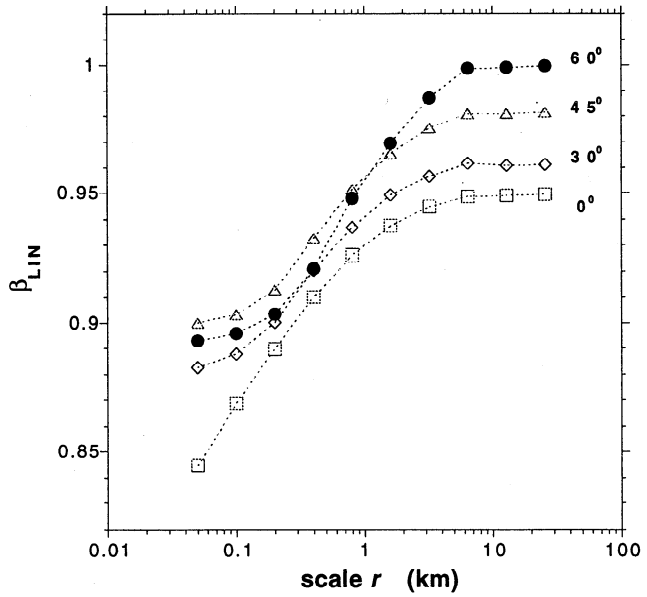

Figure 7. The effect of solar zenith angle on measurements at cloud top and cloud base. The absolute least squares slopes $\beta_{LIN}(r)$ for different solar zenith angles. Solid circles correspond to $\theta_0 = 60°$, as plotted in Figure 6a.

when clouds are not present. Thus the total photon path in clear sky ($0.3 \times \cos \theta_0$ km) between 1 and 1.3 km is roughly equal to the total path in cloudy layer of the same size while $\theta_0 = 60°$ ($\beta = 1$). When the Sun is in zenith, the clear-sky total path is much shorter than its cloudy counterpart; as a result, we have $\beta = 0.95 < 1$.

While the small-scale behavior of nonzenith Sun is similar (a more or less stable regime for scales $r < \eta \approx h$), the R versus T slope for zenith Sun shows a steep increase after the very first spatial averaging. This is because of the direct solar radiation transmitted through the small gaps "not seen" by the low-Sun photons. As a result, zenith-Sun transmittance has stronger (but thinner) spikes (outliers on the R versus T scatterplot), which are eliminated after averaging.

In summary, out of three distinct regimes found for $\theta_0 = 60°$ (Figure 6a), two regimes (a rapid increase and then the large-scale stable behavior) are robust with respect to the solar zenith angle, while the very first regime at small scales disappears as Sun approaches zenith.

6. Vertical Offset Between Aircraft

In this section we discuss the effect of vertical separation between aircraft and clouds on the slope of above cloud reflectance versus below cloud transmittance.

6.1. Linear Regression and Variability

We assume for simplicity that all uncertainties in $R(x_i)$ are identical and that the $T(x_i)$ are known exactly, that is, $\sigma_{R_i} = \sigma$ and $\sigma_{T_i} = 0$. Then in order to fit a straight line

$$R(T) = a + bT, \tag{16a}$$

we have to minimize the χ^2 merit function,

$$\chi^2(a,b) = \frac{1}{\sigma^2}\sum_{i=1}^{n}(a + bT_i - R_i)^2. \tag{16b}$$

It is easy to show [e.g., *Press et al.*, 1993] that the slope b in (16a)–(16b) is given by

$$b = \frac{1}{\mathrm{Var}(T)}\mathrm{Cov}\{T, R\}, \tag{17a}$$

where

$$\mathrm{Cov}\{T, R\} = \frac{1}{n}\sum_{i=1}^{n}(T_i - \langle T\rangle)(R_i - \langle R\rangle) = \langle (T - \langle T\rangle)(R - \langle R\rangle)\rangle, \tag{17b}$$

$$\mathrm{Var}(T) = \frac{1}{n}\sum_{i=1}^{n}T_i^2 - \left(\frac{1}{n}\sum_{i=1}^{n}T_i\right)^2 = \langle T^2\rangle - \langle T\rangle^2 \geq 0. \tag{17c}$$

If $T(x)$ is fixed and $R(x)$ is getting smoother, the absolute slope $|b|$ in the regression (16a) decreases. Indeed, in the limit case of $R(x) \equiv$ const, $R_i - \langle R\rangle \equiv 0$; hence slope $b = 0$. In general, one can show that if the differences $T_i - \langle T\rangle$ and $R_i - \langle R\rangle$ in (17b) have opposite signs (always true in the IPA), then the smaller R-range implies a smaller linear regression coefficient with respect to T in (17a). The next subsection illustrates this with the "two-aircraft" experiment for both overcast sky and broken clouds.

6.2. Effect of Vertical Offsets Between Aircraft and Clouds

We start with the overcast sky ($N = 1.000$). Figure 8a shows both reflectance and transmittance measured at 5 and 0.5 km, respectively. We see that while IPA transmittance and reflectance have similar smoothness, their MC counterparts are different; being measured 3.7 km above clouds, reflectance is smoother than transmittance measured only 0.5 km below clouds. Consequently, the absolute linear regression slope (Figure 8b) is smaller than its counterpart measured at cloud top and base. (Compare Figure 8b where $\beta_{LIN} = 0.738$ with Figure 7a where $\beta_{LIN} = 0.945$ for overcast sky.)

This effect is far more pronounced in the case of broken clouds ($N = 0.777$). Because of cloud edges, transmittance measured 0.5 km below cloud base still has sharp peaks near cloud gaps which are not smoothed (Figure 8c). By comparison, reflectance at 5.0 km is a smooth curve because of contributions from at least 260 pixels on average; thus only large-scale variability of optical depth affects the reflectance at the upper aircraft. It is not surprising that in this case the absolute least squares slope is much smaller; $\beta_{LIN} = 0.449$ in Figure 8d, while $\beta_{LIN} = 0.893$ for cloud top versus cloud base regression (Figure 4b).

Now we average both R and T as prescribed by (15); Figures 9a and 9c illustrate them averaged over $r = 6.4$ km. We see that even for broken clouds, all sharp spikes in MC transmittance are gone; MC and IPA results are similar for thick optical depths (from 30 to 50 km) and slightly shifted (by ≈ 1 km) in thin and broken regions. Quantitatively, both IPA and MC transmittances averaged over $r = 6.4$ km have the same variance,

$$\mathrm{Var}(T^{IPA}) \approx \mathrm{Var}(T^{MC}) = \begin{cases} 0.0022, & N = 1.000 \\ 0.0262, & N = 0.777 \end{cases}. \tag{18}$$

In other words, averaging over $r = 6.4$ km is sufficient to reach the IPA regime for transmittance.

MC reflectances, however, are still smoother than the IPA counterparts. Even for overcast sky (Figure 9a) we have

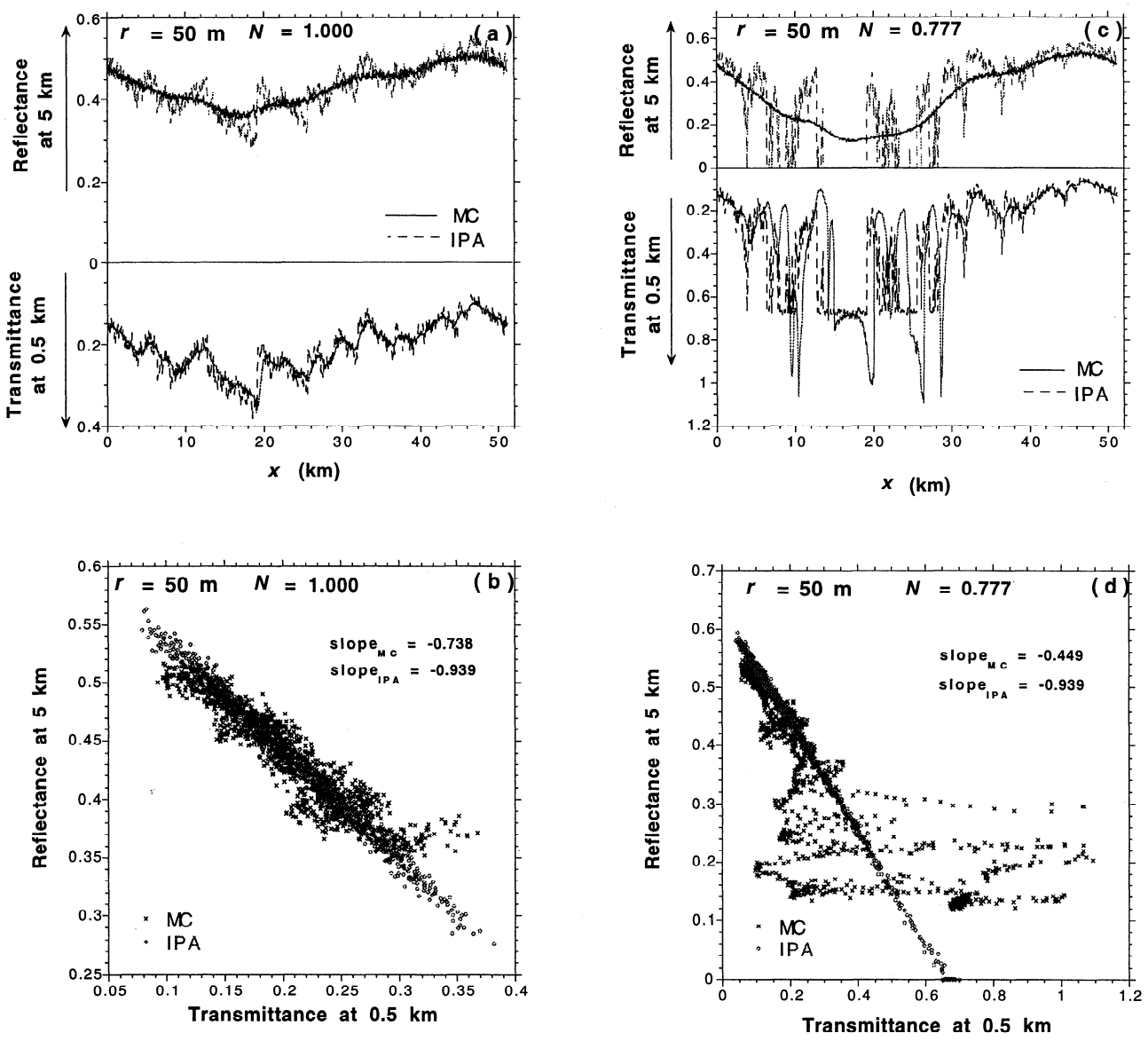

Figure 8. Reflectance at upper aircraft (5 km) and transmittance at lower aircraft (0.5 km) for overcast sky and broken clouds at smallest resolution (0.05 km). Solar zenith angle $\theta_0 = 60^o$. (a) IPA and MC fields for overcast sky. (b) Upper aircraft reflectance versus lower aircraft transmittance for overcast sky ($N = 1.000$). (c) The same as in Figure 8a but for broken clouds with $N = 0.777$. (d) The same as in Figure 8b but for broken clouds with $N = 0.777$.

$\mathrm{Var}(R^{MC}) = 0.0015$ while $\mathrm{Var}(R^{IPA}) \approx \mathrm{Var}(T^{IPA}) = 0.0022$. For broken clouds (Figure 9c), this discrepancy is more pronounced; we have $\mathrm{Var}(R^{MC}) = 0.0154$, while $\mathrm{Var}(R^{IPA}) \approx \mathrm{Var}(T^{IPA}) = 0.0262$. As a result, averaging over $r = 6.4$ km is not sufficient to bring MC reflectance to the IPA regime. Consequently, the MC slope β_{LIN} defined in (17a) is smaller than its IPA counterpart (Figures 9b and 9d).

Finally, Figure 10a illustrates the effect of vertical offsets on β_{LIN} versus scale r for overcast sky and broken clouds. In comparison to cloud top versus cloud base regressions (Figure 6a) we see that the small-scale bias between MC and IPA is substantially increased because of unequal contributions from neighboring pixels to reflectance at 5 km and transmittance at 0.5 km. However, in the case of cloud top versus cloud base regression, the small-scale bias can be removed by sufficient spatial averaging (over $20h$); the simulations with offsets above and below clouds produce an unremovable large-scale bias in the direction of increased apparent absorption. This bias is caused by smooth behavior of the MC reflectance and has nothing to do with column absorption; it indicates only that IPA regime has not been reached because of a large separation between cloud top and the upper aircraft. To summarize, as r increases, $\beta_{LIN}(r)$ converges, but to a spurious value.

Figure 10b demonstrates $\beta_{LIN}(r)$ for two reflectances at 5 and 2.3 km versus surface transmittance. The altitudes of 2.3 km and the surface were chosen to have equal offsets above and below clouds (recall that our stratiform fractal clouds are between 1 and 1.3 km). We see that in the case of equal contributions from neighboring pixels to reflectance at 2.3 km and transmittance at the surface, the large-scale bias almost disappears. In other words, a sufficient spatial averaging

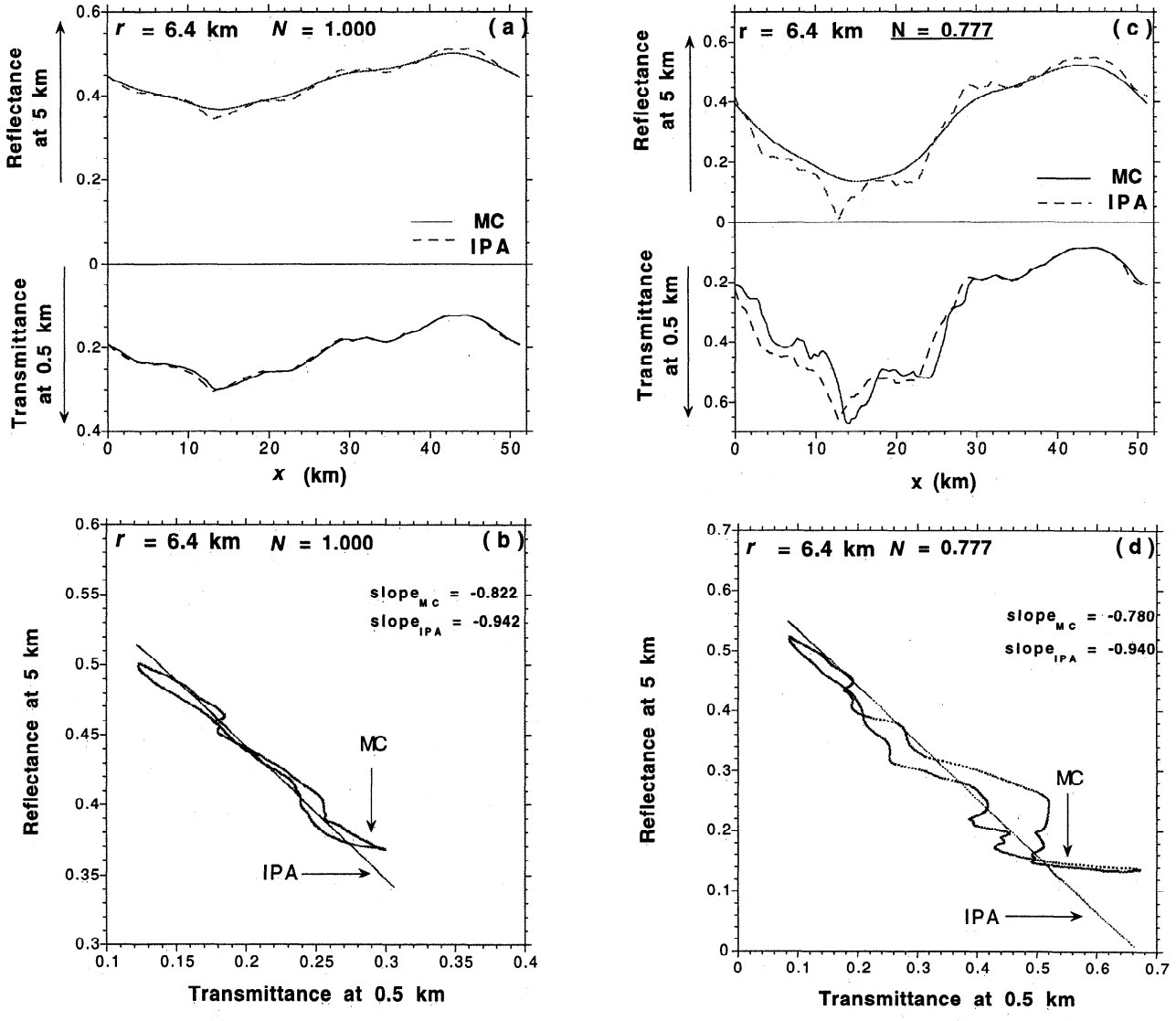

Figure 9. Spatial average (over 6.4 km) of the data in Figure 8.

brings MC results to the IPA regime, where we know $\beta_{LIN}(IPA) \approx \beta_{CF}$.

As an example, see *Marshak et al.* [1997a], where for the near-infrared wavelength with no water vapor absorption, they simulated *Hayasaka et al.*'s [1995] two-aircraft experiment and found that with the upper aircraft flying only 750 m above cloud top, spatial averaging of $\approx 30h$ was sufficient to reach the IPA regime.

6.3. Transparent Versus Opaque Spectral Bands

To separate the effect of strong water vapor absorption, two narrow (100 cm^{-1}) spectral intervals are studied independently. One of them (around 0.99 μm) is the least absorptive, while the other (around 0.94 μm) is the most absorptive interval. The least absorptive interval is almost transparent; for clear sky and $\theta_0 = 60°$, only 2% of the solar energy is absorbed between TOA and surface. For the same conditions the most absorptive (opaque) interval absorbs 80% of the incident solar energy. As a result, for the transparent band, $\beta_{CF} = 0.98$, while for the opaque one, $\beta_{CF} = 0.86$.

We know that the small-scale bias between $\beta_{LIN}(MC)$ and $\beta_{LIN}(IPA) \approx \beta_{CF}$ is due to photon horizontal transport (as for cloud top reflectance versus cloud base transmittance) and unequal contribution from neighboring pixels to reflectance above cloud top and transmittance below cloud base. If the large-scale bias is due to only water vapor absorption, the largest bias should be for the most absorptive spectral band rather than for the transparent band. Figure 11, however, indicates that the nature of the large-scale bias has little to do with water vapor absorption. More than that, the large-scale bias is larger if water vapor absorbs less; at large scales $\beta_{LIN}(IPA) - \beta_{LIN}(MC) = 0.091$ for the opaque interval, while $\beta_{LIN}(IPA) - \beta_{LIN}(MC) = 0.177$ for the transparent one. This is understandable, since strong water vapor absorption is bound to inhibit radiative smoothing processes by decreasing horizontal fluxes, hence the difference between MC and IPA for a given scale.

To summarize, the large-scale bias is a constant discrepancy between $\beta_{LIN}(MC)$ and $\beta_{LIN}(IPA)$, essentially unremovable by spatial averaging. It is due to a separation between cloud top and upper aircraft, which is not equal to that between cloud

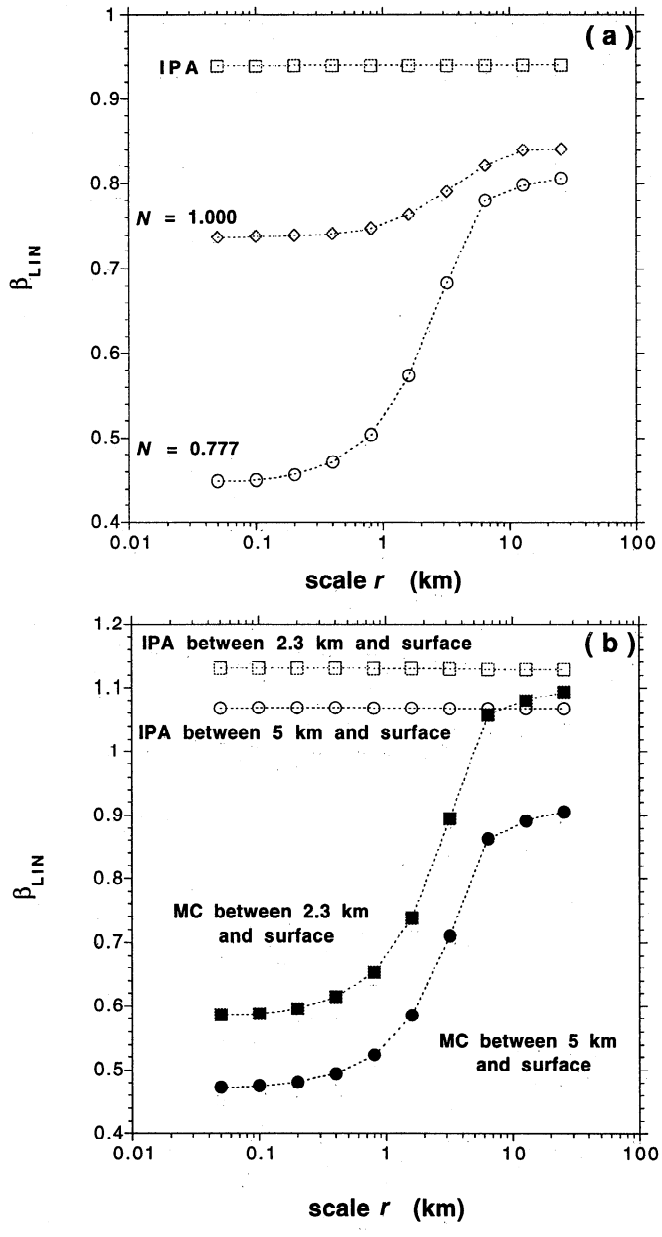

Figure 10. Linear regression of reflectance above cloud versus transmittance below cloud. Solar zenith angle $\theta_0 = 60°$. MC and IPA results. (a) Overcast sky and broken cloud with $N = 0.777$. Upper aircraft reflectance (at 5 km) versus lower aircraft transmittance (at 0.5 km). (b) Broken clouds ($N = 0.777$). Reflectance at 2.3 and 5 km versus transmittance at surface. Note that $\beta_{LIN}(IPA) \approx \beta_{CF} = 1.13$ for the upper aircraft reflectance at 2.3 km and $\beta_{LIN}(IPA) \approx \beta_{CF} = 1.07$ for the one measured at 5.0 km. This means that for $\theta_0 = 60°$ and the spectral region between 0.91 and 1.0 μm, in both cases, the removal of cloud layer leads to the increase in column absorption between upper aircraft and surface; this is more pronounced in case of upper aircraft at 2.3 km.

base and the lower aircraft. Properly chosen altitudes of measurements can reduce significantly the large-scale bias (and decrease somewhat the small-scale bias which is due to the net horizontal fluxes). An alternative way to remove net horizontal fluxes, closely related to *Ackerman and Cox*'s [1981] procedure, is discussed in the Appendix.

7. Horizontal Offset Between Aircraft

Another source of bias in estimating cloud absorption is the horizontal offset δx between two aircraft flying above and below clouds (Figure 12). We study the effect of the variability in cloud optical depth $\tau(x)$ on the linear regression $R(x)$ versus $T(x+\delta x)$, where δx is a small positive horizontal offset. We first consider the effect of δx on $\tau(x)$ and then on $T(x+\delta x)$ and estimated slope.

7.1. Scale-Invariant Optical Depth

We assume scale invariance in the horizontal distribution of optical depth, that is,

$$\langle |\tau(x+\delta x) - \tau(x)|^q \rangle \sim (\delta x/L)^{\zeta(q)}, \quad q \geq 0,\ 0 < x, x+\delta x < L,\ L \gg 0. \tag{19a}$$

For fractional Brownian motion [*Mandelbrot*, 1977], the function $\zeta(q)$ is linear,

$$\zeta(q) = qH \quad (0 \leq H \leq 1), \tag{19b}$$

while for bounded cascades used here [*Marshak et al.*, 1994],

$$\zeta(q) = \begin{cases} qH, & 0 \leq q \leq 1/H \\ 1, & 1/H \leq q \leq \infty \end{cases}. \tag{19c}$$

Parameter H in equations (19b) and (19c) is called the "roughness" or Hurst exponent; it varies from zero to unity and characterizes the smoothness of the signal. Indeed, for $q = 1$ we have $\zeta(1) = H$ and $\langle |\tau(x+\delta x) - \tau(x)|/\delta x \rangle \sim (\delta x/L)^{H-1}$; so the derivative becomes more singular as the limit $H = 0$ is approached. In contrast, the opposite limit ($H = 1$) yields almost everywhere differentiable signals. Note that $H \approx 1/3$ best fits the horizontal variability of cloud liquid water as defined by (19a) [*Cahalan et al.*, 1994a, *Davis et al.*, 1994].

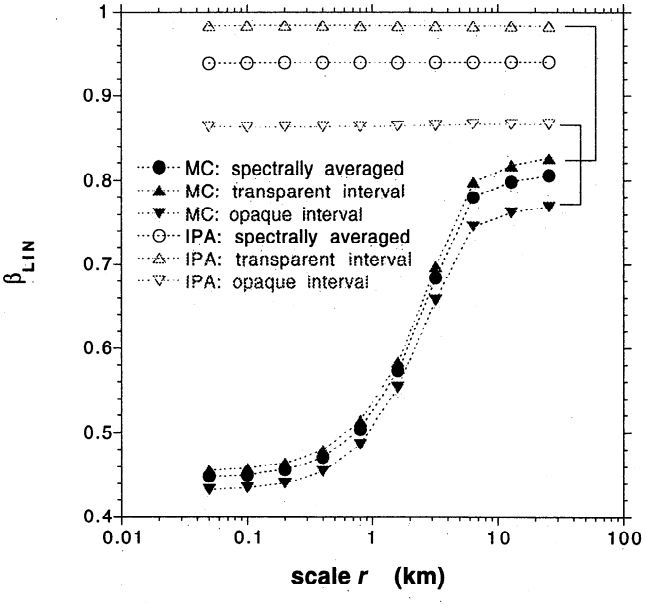

Figure 11. Linear regressions for the most and the least absorptive spectral intervals. Solar zenith angle $\theta_0 = 60°$. The upper aircraft at 5 km, the lower one at 0.5 km. $\beta_{LIN}(r)$ for the whole spectral band (between 0.91 and 1.0 μm) are plotted with the least absorptive spectral interval (around 0.99 μm) and the most absorptive one (around 0.94 μm). Scale-independent IPA results indicate the level of β_{CF}.

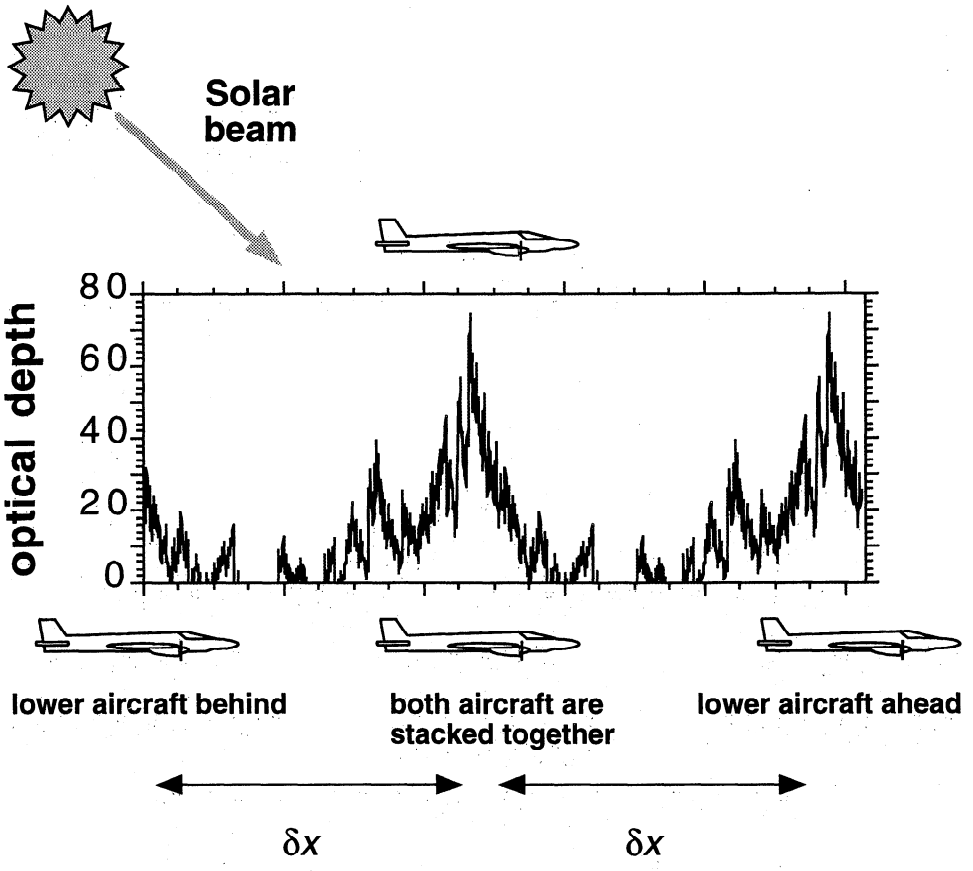

Figure 12. A schematic illustration of the horizontal offsets between aircraft.

7.2. Two-Stream Approximation

To understand the impact of the offset δx on the slope β, let us first consider the simple case of a conservative medium in the two-stream approximation [e.g., *Lenoble*, 1985],

$$R(\tau(x)) = \frac{\gamma\tau(x)}{1+\gamma\tau(x)}, \tag{20a}$$

while

$$T(\tau(x)) = \frac{1}{1+\gamma\tau(x)} \tag{20b}$$

with $\gamma = (1-g)/(2\cos\theta_0)$, where g is the scattering phase function's asymmetry factor. Note that $R = 1 - T$, so the correct value of β is unity. A little algebra yields

$$\frac{\delta R(\tau(x))}{\delta T(\tau(x+\delta x))} = -\left[\frac{1+\gamma\tau(x+\delta x)}{1+\gamma\tau(x)}\right]^2 =$$

$$-1 - \frac{2\gamma\,\delta\tau(x)}{1+\gamma\tau(x)} - \frac{\gamma^2\delta\tau(x)^2}{(1+\gamma\tau(x))^2} \tag{21}$$

where $\delta\tau(x) = \tau(x+\delta x) - \tau(x)$. Hence

$$\beta(\delta x) - 1 = 2\gamma\,\langle\delta\tau(x)T(x)\rangle + \gamma^2\langle\delta\tau(x)^2T^2(x)\rangle \tag{22a}$$

where

$$\beta(\delta x) = -\left\langle\frac{\delta R(\tau(x))}{\delta T(\tau(x+\delta x))}\right\rangle. \tag{22b}$$

Since $0 < T < 1$, we can write

$$\langle\delta\tau(x)^qT^q(x)\rangle \sim c_q\langle\delta\tau(x)^q\rangle, \quad q = 1,2 \tag{23a}$$

with c_1 and c_2 independent of δx. Then using (19a) for $q = 1$ and 2, we have

$$|1 - \beta(\delta x)| \sim c_1(\delta x/L)^{\zeta(1)} + c_2(\delta x/L)^{\zeta(2)}. \tag{23b}$$

Substituting (19c) into (23b) and neglecting the second term in the right-hand side of (23b), we get

$$|1 - \beta(\delta x)| \sim (\delta x/L)^H. \tag{24}$$

In the limit of uncorrelated optical depth we have $H = 0$, so that $\beta(\delta x) \sim 0$, $\delta x > 0$; therefore any offset between aircraft is disastrous for estimating absorption. For $H > 0$, $\beta(\delta x)$ deviates increasingly from (the correct value of) unity as either horizontal offset δx or exponent H increases.

7.3. MC and IPA Results With Horizontal Offset

Figure 13a demonstrates the effect of horizontal offset between two aircraft flying exactly at cloud top and base. The lower aircraft is ahead of the upper one (see Figure 12). Without spatial averaging, $\beta_{LIN}(\delta x)$ first slightly increases and reaches its maximum at the offset of $\delta x = h \tan\theta_0 \approx 0.5$ km when the upper and lower aircraft are along the line of solar beams. Because of net horizontal fluxes, aircraft offsets smaller than cloud thickness h have little effect on β_{LIN}. Estimates are more than 5% below the correct value unless fluxes are spatially averaged over 6.4 km or more (upper curve

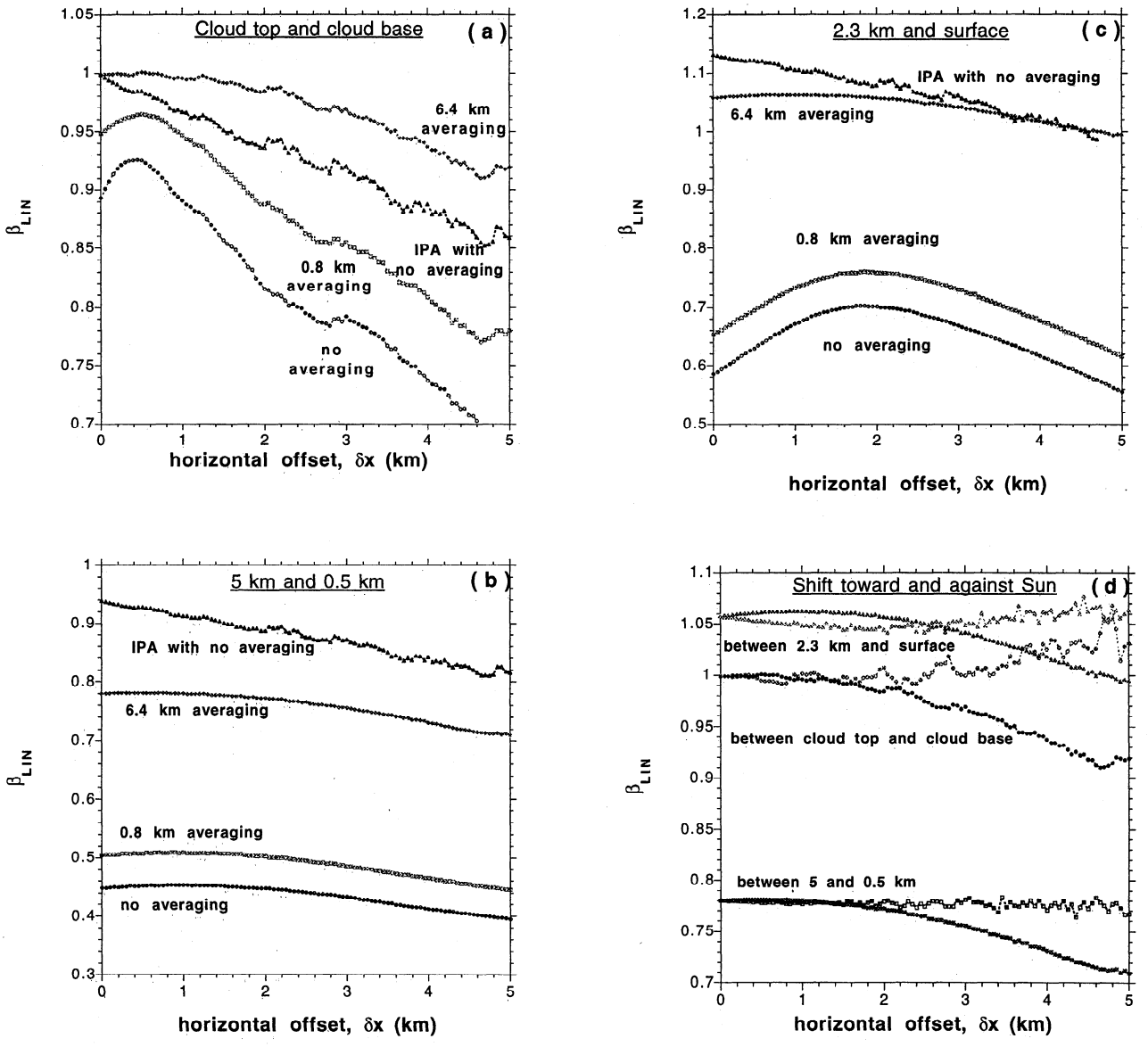

Figure 13. Effect of horizontal offset between aircraft on linear regression. Solar zenith angle $\theta_0 = 60°$. Upper aircraft is unchanged. (a) Cloud top and cloud base. Lower curve is obtained with no spatial averaging; other two curves correspond to spatially averaged reflectance and transmittance over 0.8 and 6.4 km, respectively. The IPA curve has no spatial averaging. The lower aircraft is ahead of the upper one in the direction away from the Sun. (b) The same as in Figure 13a but for reflectance at 5 km and transmittance at 0.5 km. (c) The same as in Figure 13a but for reflectance at 2.3 km and transmittance at surface. (d) The effect of horizontal offset in opposite directions as illustrated in Figure 12. Open symbols correspond to the case of the lower aircraft behind the upper one, while solid symbols correspond to the lower aircraft ahead of the upper one. The curves with the large-scale decrease (solid symbols) are the same as in Figures 13a–13c.

in Figure 13a) and the offset $\delta x \leq 3$ km. For scales larger than $h \tan \theta_0$ we are in the IPA regime, and (24) begins to describe the general functional behavior of the falling-off portion of the curves (including the IPA). As the horizontal offset increases, β_{LIN} drifts systematically away from its true value, although this drift is mitigated by spatial averaging.

For measurements between levels at 5 and 0.5 km, Figure 13b shows a relatively long stable behavior of $\beta_{LIN}(\delta x)$. However, the equidistant measurements from cloud top and base shown in Figure 13c clearly highlight the maximum at 2 km where cloud top and surface measurements are along the line of solar beams. As in case of cloud top and base measurements (Figure 13a), this maximum disappears when fluxes are spatially averaged over 6.4 km. Neither of these curves give a true value of β_{LIN}. Nevertheless, a stable and relatively accurate $\beta_{LIN}(\delta x)$ is obtained for $\delta x < 2$ km if averaged over 6.4 km in Figure 13c; this is encouraging. Thus we find that the three conditions, (1) spatial averaging over 20-30 cloud thicknesses, (2) aircraft altitudes equidistant from top and base, and (3) a reasonably small (1–2 km) horizontal offset between aircraft bring us to the IPA regime where β_{LIN} accurately estimates cloud absorption.

Finally, Figure 13d compares the effect of horizontal offsets between two different locations of the lower aircraft with

respect to the Sun and upper aircraft positions illustrated in Figure 12. We see that for fluxes spatially averaged over 6.4 km, there is little variability in $\beta_{LIN}(\delta x)$ for $\delta x < 1$–2 km. As horizontal offset increases, the drift in β_{LIN} is smaller for the case of lower aircraft behind the upper one (between 5 and 0.5 km). The opposite directions of the drift in the cloud top versus cloud base regression for large offsets may improve the overall performance when the aircraft have different speeds (as in ARESE), so that both situations happen equally often.

The above numerical experiments were conducted on a single well-defined cloud layer. In realistic two-aircraft measurements the cloud layer is often difficult to define. Thus actual application of the linear regression technique may be even more erroneous, and a 1–2 km horizontal offset between aircraft may lead to a substantial bias in a $\beta_{LIN}(\delta x)$ slope. Another weakness of the above analysis is the assumption of cyclic boundary conditions. In real-world situations, noncyclical conditions will complicate specification of minimal aircraft spacing required to achieve proper estimates.

8. Conclusion

We describe a Observation System Simulation with which "virtual" two-aircraft (as well as ground/space) experiments can be performed. On the one hand, we used it to reassess the effect of cloud inhomogeneity on *Cess et al.*'s [1995] method of estimating cloud-induced shortwave absorption using reflectance (R) versus transmittance (T) regressions. On the other hand we revisited *Ackerman and Cox*'s [1981] idea of using multiple spectral channels to remove the effect of horizontal fluxes from two-aircraft measurements of column absorption.

8.1. Observation System Simulation

A fractal model of optical depth appropriate for marine boundary layer clouds is used. Clear-sky gaps are added in an empirical way to simulate the effect of cloud edges. All simulated clouds have the same total amount of liquid water and the corresponding domain-averaged optical depth is 13, while cloud thickness is held constant at 0.3 km; pixels are 50 m wide, and the computational domain (1024 pixels) is 51 km. A narrow spectral band from 0.9 to 1.0 μm, characterized by strong water vapor absorption and weak cloud liquid water absorption, is selected for a detailed study. Two numerical approaches are used for the radiative transfer: (1) the independent pixel approximation (IPA) which accounts for the horizontal distribution of optical depth but ignores any net horizontal fluxes; and (2) the Monte Carlo (MC) method which accounts exactly for the net horizontal fluxes. In another study [*Marshak et al.*, 1997b] we establish that for the domain-averaged column absorption (the targeted quantity in all current experiments) the IPA accounts for effect of horizontal variability to within 2% of the absorptance or better.

Our cloud models are geometrically plane-parallel, single-layered, and variable in only one horizontal direction, and we use cyclical boundary conditions. In a more realistic situation with 3-D variability, including nonflat cloud boundaries [cf. *Evans*, 1997; Barker and Li, submitted manuscript, 1997], our estimations of sufficient averaging should actually be viewed as lower bounds.

8.2. Ackerman-Cox Correction

We found that 3-D radiative transfer effects can be removed from a two-aircraft record, without degrading the spatial resolution, by using a modified version of the Ackerman-Cox procedure. By subtracting apparent absorption for the quasitransparent narrow sub-band around 0.99 μm, with an appropriate weight, from its counterpart obtained by averaging over the whole 0.9–1.0 μm spectral region, we can restore an IPA-type field where photon horizontal transport plays almost no role. The weight for the modified correction is uniquely determined through linear regression of $A(x)_{whole}$ versus $A(x)_{transparent}$, where x is the horizontal coordinate [*Titov*, 1997].

8.3. Cloud Variability Effects in Column Absorption via R Versus T Regression

This method, introduced by *Cess et al.* [1995], yields a linear regression slope β_{LIN}. Another method, introduced by *Ramanathan et al.* [1995] uses cloud forcing ratio β_{CF} which is based on overall spatial averages rather than a least squares fit but requires a clear-sky identification. The former approach, while showing identical results ($\beta_{CF} = \beta_{LIN}$) for R and T values from general circulation model (GCM) radiation modules, may be quite different or even uncertain in the case of real measurements [*Imre et al.*, 1996, *Arking et al.*, 1996; *Li and Moreau*, 1996; Barker and Li, submitted manuscript, 1997]. This was our primary motivation when developing the Observation System Simulation and we summarize our main findings below.

Our prototype of a GCM radiation scheme is the IPA, and Figure 3 shows that we indeed have $\beta_{CF} \approx \beta_{LIN}$ for different measurement altitudes. From the other side, MC fluxes are our surrogates for real measurements; they always give $\beta_{LIN} < \beta_{CF}$ (Figure 6a). This is due to the effect of net horizontal fluxes, which we hold as the major source of systematic bias in cloud absorption estimates based on two aircraft and the R versus T method. If measured exactly at cloud top and base and the aircraft are perfectly stacked, the bias can be eliminated by sufficient spatial averaging (see (14) and (15) and Figures 6a, 6b, and 7]. The characteristic scale here is essentially the cloud thickness. Spatial averaging over horizontal distances several times the vertical cloud thickness is necessary to reach the IPA regime where the net horizontal fluxes can be neglected. Averaging over a horizontal scale smaller than the cloud thickness gives a slope β_{LIN} much smaller than the one estimated from IPA results and thus a falsely large "apparent cloud absorption."

Different cloud fractions (Figure 6c) and solar angles (Figure 7) can change substantially the small-scale slope but do not affect much the amount of spatial averaging required to remove the absorption bias. We find the required scale to be insensitive to both solar angle and cloud fractions and equal to about 20–30 cloud thicknesses. This is encouraging, since it allows us to apply the same algorithm of spatial averaging to all data obtained during several hours of measurement.

Spatial averaging, however, does not always lead to the "true" IPA regime. If the separation between upper aircraft and cloud top is large enough, the reflectance is much smoother than the transmittance; as a result, β_{LIN} converges to a spuriously low value (Figure 10a) which again gives a falsely large apparent absorption. This estimate moves further from

the correct value as the upper aircraft increases in altitude above the cloud top.

Performance of the R versus T method for two aircraft measurements can be improved if proper altitudes for both aircraft are found (Figure 10b). The ideal case is to fly exactly at cloud top and base; this has the additional advantage of focusing on "in-cloud" absorption, as opposed to "column" absorption in the presence of clouds. If this is impractical, at least the contribution from neighboring pixels should be similar for both reflectance and transmittance measurements. Since the lower aircraft is limited by the ground, it is recommended to fly the upper aircraft above the cloud top equal to the distance between cloud base and surface.

The horizontal offsets between two aircraft are also detrimental if not properly accounted for. If the IPA regime is reached by sufficient spatial averaging (tens of cloud thicknesses), a horizontal offset of a few cloud thicknesses does not affect β_{LIN}. If horizontal offset increases beyond several km, β_{LIN} drifts from the true (IPA) value and falsely indicates a large apparent absorption.

The R versus T scatterplot is only one of several methods estimating the effect of clouds on atmospheric absorption [*Ramanathan et al.*, 1995; *Cess et al.*, 1995], and *Imre et al.* [1996] showed that, so far, none of them is completely satisfactory. Indeed, their sensitivities to clear-sky identification, solar zenith angle, water vapor distribution, surface condition, choice of measurement levels, amount of spatial averaging, and many others factors complicate the characterization of true cloud absorption. In the present study we analyzed the implementation of the R versus T method to estimate column absorption between two vertical levels in the 0.9–1.0 μm spectral region and found that sufficient spatial averaging removes 3-D effects and a well-designed two-aircraft experiment can give reasonable results.

Appendix: A Modified Ackerman-Cox Correction

Ackerman and Cox [1981] analyzing the aircraft data during the Summer Monsoon Experiment, suggested to correct absorption in the near-infrared spectral region by subtracting apparent absorption in the visible region. Their justifications are based on the two main assumptions: (1) there is no in-cloud absorption in the visible spectral region and (2) in units of incident flux, 3D effects in the near-infrared spectral region are roughly equal to those in the visible region. As a result, pixel-by-pixel subtraction of the apparent visible region absorption will remove 3-D radiative transfer effects in the observed flux differences in the near-infrared region.

Hayasaka et al. [1995] applied the Ackerman-Cox correction both to dual-aircraft measurements in the North Pacific Ocean and to MC calculations; they found a good agreement between the measured absorptance of inhomogeneous clouds and that obtained by MC. *Ramanathan and Vogelmann* [1997], however, noted that atmosphere is not strictly nonabsorbing in the visible region and the data averaged over tens of individual clouds will, in all likelihood, capture photons leaking through cloud edges. Instead, they suggested to include the 3-D effects in models, to compute the resulting absorption and compare these with unadjusted measurements.

Since we have an almost non-absorbing subinterval around 0.99 μm in the 0.91–1.0 μm spectral band, we can apply the

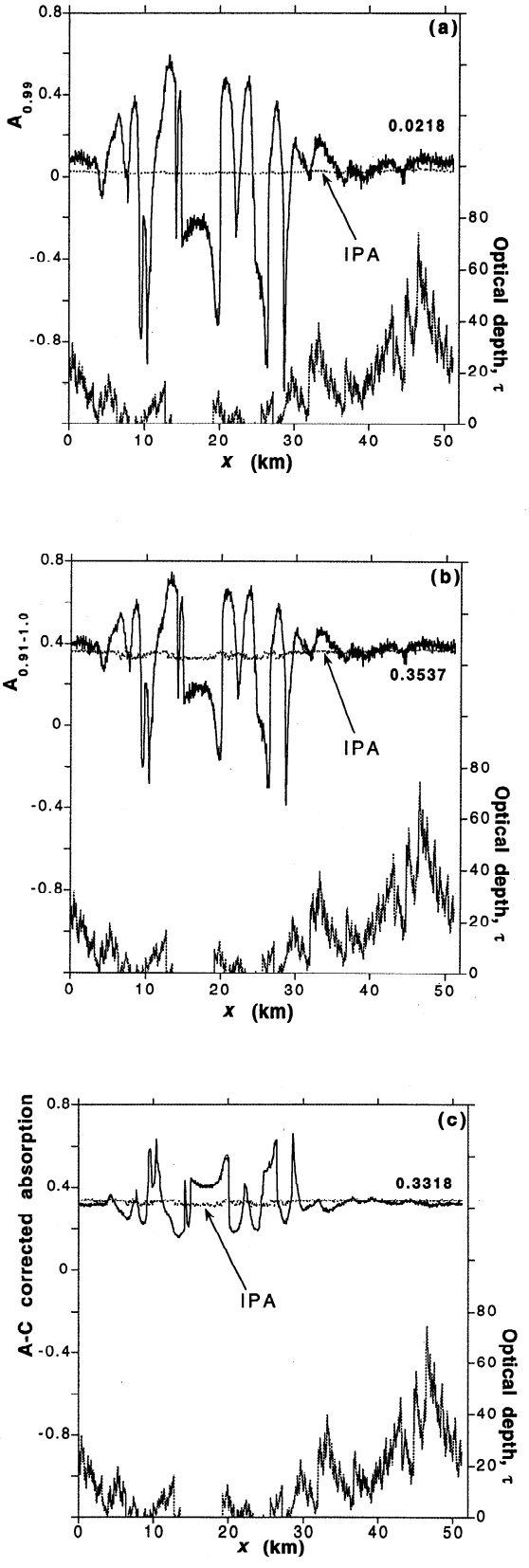

Figure A1. Ackerman-Cox type correction. Solar zenith angle $\theta_0 = 60°$. MC and IPA column absorptions between two vertical layers above and below clouds. Optical depth distribution $\tau(x)$ is added for reference. (a) Almost transparent narrow spectral band around 0.99 μm. (b) Averaged over the whole spectral interval 0.91–1.0 μm. (c) Differences between Figures A1b and A1a.

Ackerman-Cox correction using this subinterval as a prototype of the visible region while the whole 0.91–1.0 μm spectral interval as a prototype of the near-infrared region. Note that between two altitudes of 0.5 and 5 km and for solar zenith angle $\theta_0 = 60^o$ the nonabsorbing subinterval absorbs about 2%, while the whole 0.91–1.0 μm spectral interval absorbs about 35% of solar energy that reaches 5 km altitude.

Figure A1a shows apparent absorption in the subinterval around 0.99 μm. Because of cloud edges the range of (almost purely apparent) column absorption is spread from -0.9 to 0.6, having only 0.022 on average.

The whole 0.91–1.0 μm spectral interval column absorption is plotted in Figure A1b and we see that it looks like a shifted and squeezed version of that in Figure A1a. Indeed, we still see negative apparent absorption values and the range is from -0.4 to 0.75. This field shows a deficit of absorption for clear-sky regions (e.g., around $x = 15$ km, $x = 24$ km), which is compensated by enhanced absorption at cloud edges. (*Davis et al.* [1997c] propose an analytical diffusion-based model for this 3-D radiative transfer process that parallels the theory of flow through porous media.)

Figure A1c illustrates the corrected absorption field,

$$A_{\mathrm{AC_{cor}}}(x) = A(x)_{0.91\text{–}1.0} - A(x)_{0.99}, \tag{A1}$$

which is less variable than $A(x)_{0.91\text{–}1.0}$ plotted in Figure A1b; it does not have any negative absorption, and both IPA (added for comparison) and MC fields in the unbroken parts of our cloud model are very close. On the other hand, the clear sky regions show enhanced absorption which is compensated by the deficit at cloud edges. To summarize, the Ackerman-Cox correction certainly reduces the range of $A(x)_{0.91\text{–}1.0}$ field, but instead of removing the 3-D effects it overcompensates for them.

Let us now weaken the second Ackerman-Cox assumption. We assume that 3-D effects in the near-infrared and visible spectral regions are just linearly related; that is,

$$A(x)_{0.91\text{–}1.0} = d + c\,A(x)_{0.99}; \tag{A2}$$

previously, we had $c = 1$. Thus, instead of (A1) we have

$$A_{\mathrm{LIN_{cor}}}(x) = A(x)_{0.91\text{–}1.0} - c\,A(x)_{0.99} \tag{A3}$$

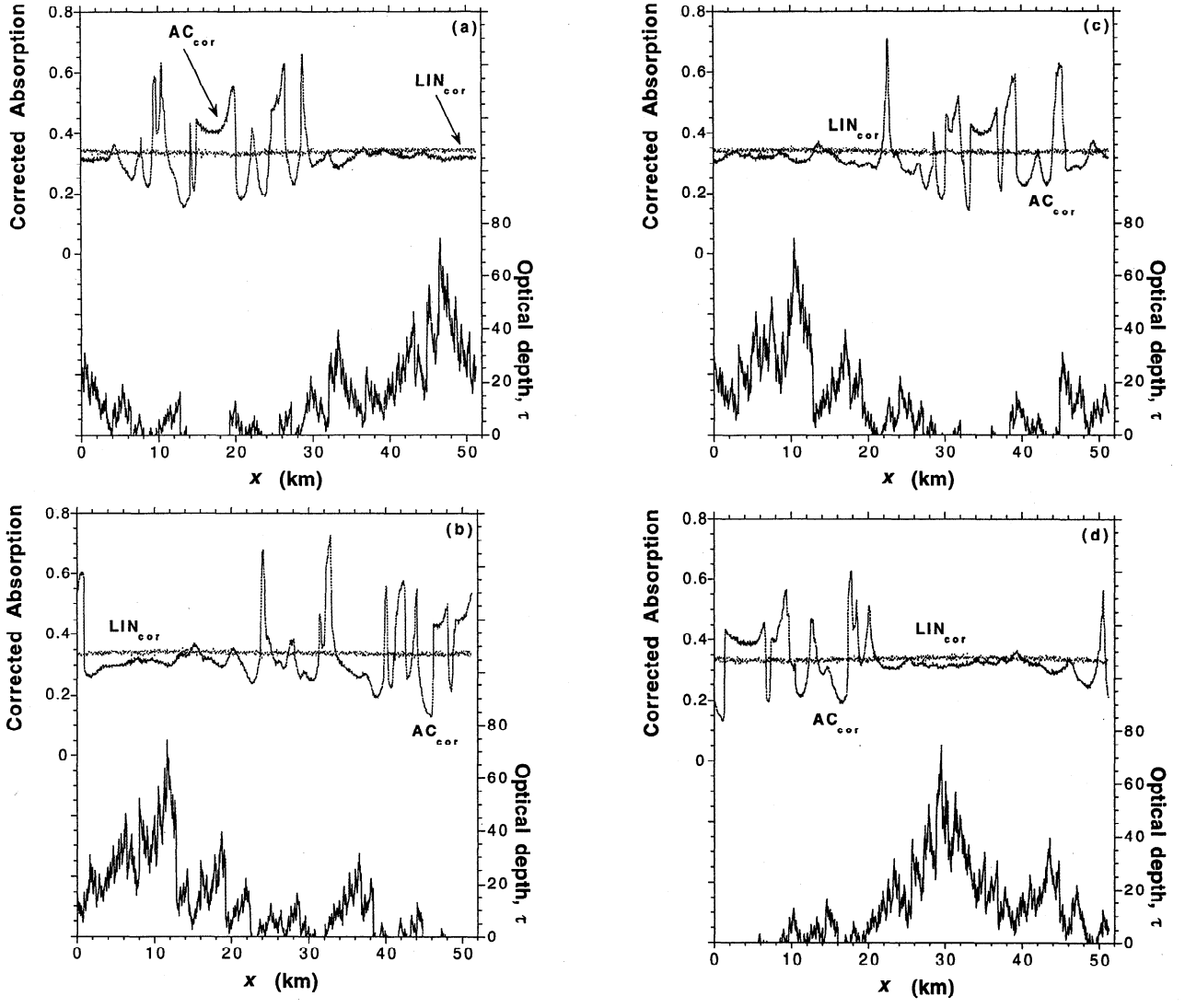

Figure A2. Modified Ackerman-Cox correction for column absorption. Four realizations of the bounded cascade model, solar zenith angle $\theta_0 = 60^o$. Ackerman-Cox correction defined by (A1) is plotted together with the linear correction defined in (A3).

where suffix $\mathrm{LIN_{cor}}$ stands for linear correction and constant $c \leq 1$ is determined as a linear regression $A_{0.91-1.0}$ versus $A_{0.99}$; that is,

$$c = \left\langle \frac{\delta A_{0.91-1.0}}{\delta A_{0.99}} \right\rangle_{\text{least squares}}. \quad \text{(A4)}$$

Note that if first assumption is valid, then

$$\langle A_{0.99} \rangle \approx 0 \quad \text{(A5a)}$$

and

$$\langle A_{\mathrm{LIN_{cor}}} \rangle \approx \langle A_{\mathrm{AC_{cor}}} \rangle \approx \langle A_{0.91-1.0} \rangle, \quad \text{(A5b)}$$

independently of c.

Linear regression $A(x)_{0.91-1.0}$ versus $A(x)_{0.99}$, defined in (A4), yields $c \approx 0.7$. Figure A2a shows two absorption fields corrected using (A1) and (A3) with $c \approx 0.7$ respectively. The latter field is almost a constant and indistinguishable visually from the corresponding IPA; that is, 3-D radiative transfer effects are removed.

Coefficient c is apparently insensitive to the horizontal distribution of optical depth. To confirm this, we simulated three other realizations of optical depth fields using a bounded cascade model. Plotting apparent absorption $A(x)_{0.91-1.0}$ versus $A(x)_{0.99}$ for each realization, we find that $c = 0.68 \pm 0.02$. Figures A2a–A2d show that $A_{\mathrm{LIN_{cor}}}(x)$ for all four realizations of cloud model is essentially independent of x. From the other side, we can relate $A_{\mathrm{LIN_{cor}}}(x)$ to the IPA column absorption, which also ignores horizontal fluxes.

The uniqueness of c comes primarily from the fact that phase functions and single-scattering albedos in the transparent spectral band around 0.99 μm are similar to those in the whole spectral interval 0.91–1.0 μm. It is not yet clear how (A3) will work for the whole near-infrared and visible spectral regions; this issue will be addressed elsewhere [see also *Titov*, 1997].

Acknowledgments. This work was supported by the Environmental Sciences Division of U.S. Department of Energy (under grant DE-A105-90ER61069 to NASA's Goddard Space Flight Center) as part of the Atmospheric Radiation Measurement (ARM) program. We especially thank W. Ridgway for providing us with *k*-distribution and the results of line-by-line calculations for plane-parallel clouds. We thank A. Arking, H. Barker, R. Cess, M.-D. Chou, C. Gautier, Z.-Q. Li, W. O'Hirok, R. Pincus, G. Titov, F. Valero, and B. Wielicki for stimulating discussions.

References

Ackerman, S. A., and S. K. Cox, Aircraft observations of the shortwave fractional absorptance of non-homogeneous clouds, *J. Appl. Meteor.*, *20*, 1510–1515, 1981.

Arking, A., Absorption of solar energy in the atmosphere: discrepancy between model and observations, *Science*, *273*, 779–782, 1996.

Arking, A., M.-D. Chou, and W. L. Ridgway, On estimating the effect of clouds on atmospheric absorption based on flux observations above and below cloud level, *Geoph. Res. Let.*, *23*, 829–832, 1996.

Barker, H., A spectral analysis of albedo and bidirectional reflectances for inhomogeneous clouds, *Remote Sens. Envir.*, *54*, 113–120, 1995.

Byrne, R. N., R. C. Somerville, and B. Subasilar, Broken-cloud enhancement of solar radiation absorption, *J. Atmos. Sci.*, *53*, 878–886, 1996.

Cahalan, R. F., Overview of fractal clouds, in *Advances in Remote Sensing Retrieval Methods*, pp. 371–388, A. Deepak, Va., 1989.

Cahalan, R. F., W. Ridgway, W. J. Wiscombe, T. L. Bell, and J. B. Snider, The albedo of fractal stratocumulus clouds, *J. Atmos. Sci.*, *51*, 2434–2455, 1994a.

Cahalan, R. F., W. Ridgway, W. J. Wiscombe, S. Golmer, and Harshvardhan, Independent pixel and Monte Carlo estimates of stratocumulus albedo, *J. Atmos. Sci.*, *51*, 3776–3790, 1994b.

Cess, R. D., et al., Absorption of solar radiation by clouds: Observations versus models, *Science*, *267*, 496–499, 1995.

Cess, R. D., M. H. Zhang, Y. Zhou, X. Jing, and V. Dvortsov, Absorption of solar radiation by clouds: Interpretations of satellite, surface and aircraft measurements, *J. Geophys. Res.*, *101*, 23299–23309, 1996.

Davis, A., A. Marshak, W. Wiscombe, and R. Cahalan, Multifractal characterizations of non-stationarity and intermittency in geophysical fields: Observed, retrieved, or simulated, *J. Geophys. Res.*, *99*, 8055–8072, 1994.

Davis, A., A. Marshak, R. Cahalan, and W. Wiscombe, The LANDSAT scale-break in stratocumulus as a three-dimensional radiative transfer effect, implications for cloud remote sensing, *J. Atmos. Sci.*, *54*, 241–260, 1997a.

Davis, A., A. Marshak, W. Wiscombe, and R. Cahalan, Evidence for net horizontal radiative fluxes in marine stratocumulus, in *IRS'96: Current Problems in Atmospheric Radiation*, edited by W. L. Smith and K. Stamnes, pp. 809–812, A. Deepak, Hampton, Va., 1997b.

Davis, A., A. Marshak, W. Wiscombe, and R. Cahalan, Insight into three-dimensional radiation transport processes from diffusion theory, in *Proceedings of RADIATION'97 – An International Symposium on Radiative Transfer*, Begell House, Inc., in press, 1997c.

Davis, A., D. M. Winker, A. Marshak, J. D. Spinhirne, R. F. Cahalan, S. Love, S. H. Melfi, and W. J. Wiscombe, Retrieval of physical and optical cloud thicknesses from space-borne and wide-angle lidar, in *Advances in Atmospheric Remote Sensing with Lidar*, edited by A. Ansmann, R, Neuber, P. Rairoux, and U. Wadunger, pp. 193–196, Springer-Verlag, 1997d.

Evans, K. F., The spherical harmonic discrete ordinate method: application to 3D radiative transfer in boundary layer clouds, in *IRS'96: Current Problems in Atmospheric Radiation*, edited by W. L. Smith and K. Stamnes, pp. 143–146, A. Deepak, Hampton, Va., 1997.

Harshvardhan, W. Ridgway, V. Ramaswamy, S. M. Freidenreich, and M. Batley, Solar absorption in cloudy atmosphere, in *Seventh Symposium on Global Change Studies*, pp. 127–134, Boston, Ma, 1996.

Hayasaka, T., N. Kikushi, and M. Tanaka, Absorption of solar radiation by stratocumulus clouds: Aircraft measurements and theoretical calculations, *J. Appl. Meteorol.*, *34*, 1047–1055, 1995.

Imre, D. G., E. H. Abramson, and P. H. Daum, Quantifying cloud-induced shortwave absorption: An estimation of uncertainties and of recent arguments for large excess absorption, *J. Appl. Meteor.*, *35*, 1991–2010, 1996.

Lenoble, J. (Ed.), *Radiative Transfer in Scattering and Absorbing Atmospheres: Standard Computational Procedures*, 300 pp, A. Deepak, Hampton, Va., 1985.

Li, Z.-Q., H. W. Barker, and L. Moreau, The variable effect of clouds on atmospheric absorption of solar radiation, *Nature*, *376*, 486–490, 1995.

Li, Z.-Q., and L. Moreau, Alteration of solar absorption by clouds: simulation and observation, *J. Appl. Meteorol.*, *35*, 653–670, 1996.

Mandelbrot, B. B., *Fractals: Form, Chance, and Dimension*, 365 pp., W. H. Freeman, New York, 1977.

Marshak, A., A. Davis, R. Cahalan, and W. Wiscombe, Bounded cascade models as non-stationary multifractals, *Phys. Rev. E Stat. Phys. Plasmas Fluids Relat. Interdiscip. Top.*, *49*, 55–69, 1994.

Marshak, A., A. Davis, and W. Wiscombe, 1995: Radiation smoothing in fractal clouds. *J. Geophys. Res.*, *100*, 26247–26261.

Marshak, A., A. Davis, W. Wiscombe, and R. Cahalan, The effect of horizontal fluxes on cloud absorption estimates based on simulated two-aircraft measurements of fractal clouds, in *IRS'96: Current Problems in Atmospheric Radiation*, edited by W. L. Smith and K. Stamnes, pp. 415–418, A. Deepak, Hampton, Va., 1997a.

Marshak, A., A. Davis, W. Wiscombe, and W. Ridgway, Biases in shortwave column absorption in the presence of fractal clouds, *J. Climate*, in press, 1997b.

Marchuk, G., G. Mikhailov, M. Nazaraliev, R. Darbinjan, B. Kargin, and B. Elepov, *The Monte Carlo Methods in Atmospheric Optics*, 208 pp., Springer-Verlag, New York, 1980.

O'Hirok, W., and C. Gautier, The role of three-dimensional clouds on atmospheric absorption, *J. Atmos. Sci.*, in press, 1997.

Pilewskie, P., and F. P. Valero, Direct observations of excess solar absorption by clouds, *Science*, *267*, 1626–1629, 1995.

Press, W. H., S. A. Teukolsky, W. T. Vetterling, and B. P. Flannery, *Numerical Recipies in FORTRAN*, 2nd ed., Cambridge Univ. Press, New York, 1993.

Ramanathan, V., B. Subasilar, G. J. Zhang, W. Conant, R. D. Cess, J. T. Kiehl, G. Grassl, and L. Shi, Warm pool heat budget and short-wave cloud forcing: A missing physics? *Science*, *267*, 499–503, 1995.

Ramanathan, V., and A. M. Vogelmann, Greenhouse effect, atmospheric solar absorption and the Earth's radiation budget: From the Arrhenius-Langley Era to the 1990s, *Ambio*, 26, 38-46, 1997.

Titov, G. A. Radiative horizontal transport and absorption by stratocumulus clouds, *J. Atmos. Sci.*, in press, 1997.

R. Cahalan, A. Davis, A. Marshak, and W. Wiscombe, NASA Goddard Space Flight Center, MC 913, Greenbelt, MD 20771. (e-mail: cahalan@clouds.gsfc.nasa.gov; davis@climate.gsfc.nasa.gov; marshak@climate.gsfc.nasa.gov; wiscombe@climate.gsfc.nasa.gov)

(Received January 16, 1997; revised April 2, 1997; accepted April 16, 1997.)